Article:
Kolo, I. and de Borst, R. (2018) Dispersion and isogeometric analyses of second-order and fourth-order implicit gradient-enhanced plasticity models. International Journal for Numerical Methods in Engineering, 114 (4). pp. 431-453. ISSN: 0029-5981

https://doi.org/10.1002/nme.5749

INTERNATIONAL JOURNAL FOR NUMERICAL METHODS IN ENGINEERING
Int. J. Numer. Meth. Engng 2017; **00**:1–30
Published online in Wiley Online Library (www.onlinelibrary.wiley.com). DOI: 10.1002/nme.5749

Dispersion and isogeometric analyses of second-order and fourth-order implicit gradient-enhanced plasticity models

Isa Kolo and René de Borst*

Department of Civil and Structural Engineering, University of Sheffield, Sheffield S1 3JD, UK

SUMMARY

Implicit gradient plasticity models incorporate higher-order spatial gradients via an additional Helmholtz type equation for the plastic multiplier. So far, the enrichment has been limited to second-order spatial gradients, resulting in a formulation that can be discretised using $\mathcal{C}^0$-continuous finite elements. Herein, an implicit gradient plasticity model is formulated which includes a fourth-order gradient term as well. A comparison between the localisation properties of both implicit gradient plasticity formulations and the explicit second-order gradient plasticity model is made using a dispersion analysis. The higher-order continuity requirement for the fourth-order implicit gradient plasticity model has been met by exploiting the higher-order continuity property of isogeometric analysis, which uses NURBS as shape functions instead of Lagrange polynomials. The discretised variables, displacements and plastic multiplier, may require different orders of interpolation, an issue which is also addressed. Numerical results show that both formulations can be used as localisation limiter, but that quantitative differences occur, and a different evolution of the localisation band is obtained for two-dimensional problems. Copyright © 2017 John Wiley & Sons, Ltd.

Received . . .

KEY WORDS: Implicit gradient plasticity; higher-order continuum; isogeometric analysis; NURBS; dispersion analysis

1. INTRODUCTION

Softening caused by inherent microstructural defects can lead to the formation of localisation bands. Constitutive modelling of this process in the framework of standard continuum plasticity leads to ill-posed problems, which feature unphysical solutions with a vanishing energy dissipation upon refinement of the discretisation. This can be considered as a consequence of the absence of an internal length scale, which causes the localisation band to have a zero width.

This mesh sensitivity is removed when incorporating a length scale in the material description. Often, standard continuum plasticity is enhanced by replacing quantities like the inelastic strain by weighted averages (nonlocal theories) or by adding higher-order gradients of an internal variable such as the accumulated plastic strain (gradient theories). Doing so, a continuum description can ensue which allows for localised solutions, while preserving well-posedness of the boundary value problem [1, 2, 3, 4, 5].

*Correspondence to: René de Borst, Department of Civil and Structural Engineering, University of Sheffield, Sheffield S1 3JD, UK. E-mail: r.deborst@sheffield.ac.uk

In nonlocal models, volume integrals have to be computed at every material point. This can make such models numerically inefficient, which provides a rationale for developing gradient approximations [6, 7, 8, 9]. Indeed, gradient regularisation can also be considered as an approximation of a fully nonlocal, integral-type model. When a truncated Taylor series of the averaged quantity is substituted in a nonlocal model, a gradient formulation can be derived [9, 10, 11]. It is important to note that the approximation of the nonlocal variable can be based on either the higher-order derivatives of the local variable (explicit formulation), or on the nonlocal variable (implicit formulation).

Early studies in plasticity focused on an explicit gradient enhancement, which usually requires $\mathcal{C}^1$-continuity of the shape functions [3]. It has been attempted to satisfy this requirement using Hermitian finite elements [12], using meshless methods [13], and recently, isogeometric analysis [14]. The ability of this explicit gradient plasticity model, in which the yield stress is made a function of the Laplacian of the accumulated plastic strain in addition to the plastic strain itself, to fully regularise the boundary value problem has been demonstrated through one-dimensional dispersion analysis [15], spectral analyses [16, 17, 18], and shear band simulations [12, 13].

On the other hand, implicit gradient plasticity models with second-order gradients do not fully regularise the boundary-value problem, as has been demonstrated through spectral analysis [16, 17, 19] and three-dimensional simulations [17]. Two approaches have been identified to improve this situation, namely the use of a multiplicative yield function with a damage term, and over-nonlocal implicit gradient plasticity [16, 19, 20]. The localisation properties of both methods have been analysed using one-dimensional spectral analysis and the latter approach has been scrutinised whether it can produce shear-band which are mesh-objective [17]. It is noted that the multiplicative yield function proposed in [8] can be conceived as a special case of the over-nonlocal formulation which is a linear combination of the local and non-local history variable. In this context, the ratio of the local and non-local moduli determines whether regularisation is achieved or not [20, 21].

The practical use of implicit gradient plasticity models derived from nonlocal averaging seems to be limited to a Taylor series truncated after the second-order gradient [8, 21]. This can be partly attributed to the fact that the ensuing formulation represents a special case of the nonlocal model when an appropriate (Green's) weighting function is adopted [8, 10]. Perhaps more importantly, the formulation requires only $\mathcal{C}^0$-continuity of the shape functions, which is compatible with standard finite elements. However, the inclusion of fourth-order gradients requires $\mathcal{C}^1$-continuity of shape functions, which results in the same continuity requirements as an explicit second-order enrichment, with the computational inconveniences that come with it. Herein, we consider inclusion of second-order gradients as well as fourth-order gradients. Higher-order continuity is achieved using higher-order NURBS shape functions within the context of isogeometric analysis [22].

This paper expounds the formulation and implementation of implicit gradient-enhanced plasticity models, exploiting isogeometric analysis. The implicit gradient plasticity formulations are presented first. Next, a one-dimensional dispersion analysis is carried out to study the localisation properties of different formulations. The isogeometric finite element discretisation of the field equations is outlined and the interpolation requirements for the discretised variables are highlighted. Bézier extraction [23] is employed to arrive at a standard finite element data structure. One-dimensional simulations and two-dimensional shear band simulations further illustrate the responses of both formulations.

2. IMPLICIT GRADIENT-ENHANCED PLASTICITY

2.1. Incremental boundary value problem

We consider the equilibrium equation:

$$\mathbf{L}^{\mathrm{T}}\boldsymbol{\sigma} = \mathbf{0} \tag{1}$$

where $\boldsymbol{\sigma} = [\sigma_{xx}, \sigma_{yy}, \sigma_{zz}, \sigma_{xy}, \sigma_{yz}, \sigma_{zx}]^{\mathrm{T}}$ is the stress vector, and $\mathbf{L}$ is the differential operator:

$$\mathbf{L} = \begin{bmatrix} \frac{\partial}{\partial x} & 0 & 0 & \frac{\partial}{\partial y} & \frac{\partial}{\partial z} & 0 \\ 0 & \frac{\partial}{\partial y} & 0 & \frac{\partial}{\partial x} & 0 & \frac{\partial}{\partial z} \\ 0 & 0 & \frac{\partial}{\partial z} & 0 & \frac{\partial}{\partial x} & \frac{\partial}{\partial y} \end{bmatrix}^{\mathrm{T}}. \tag{2}$$

Under the assumption of small displacement gradients, the following kinematic relation holds:

$$\boldsymbol{\varepsilon} = \mathbf{L}\mathbf{u} \tag{3}$$

with the strain vector $\boldsymbol{\varepsilon} = [\varepsilon_{xx}, \varepsilon_{yy}, \varepsilon_{zz}, \tau_{xy}, \tau_{yz}, \tau_{zx}]^{\mathrm{T}}$ and the displacement vector $\mathbf{u} = [u_x, u_y, u_z]^{\mathrm{T}}$. The incremental constitutive relation between the stress and strain increments is given by:

$$\mathrm{d}\boldsymbol{\sigma} = \mathbf{D}^e(\,\mathrm{d}\boldsymbol{\varepsilon} - \mathrm{d}\boldsymbol{\varepsilon}^p) \tag{4}$$

where $\mathbf{D}^e$ is the material elastic stiffness matrix and $\mathrm{d}\boldsymbol{\varepsilon}^p$ is the plastic strain increment vector. An associated plasticity flow rule is adopted:

$$\mathrm{d}\boldsymbol{\varepsilon}^p = \mathrm{d}\lambda\mathbf{m}, \quad \mathbf{m} = \frac{\partial F}{\partial \boldsymbol{\sigma}} \tag{5}$$

in which $\mathrm{d}\lambda$ is a non-negative plastic multiplier and $\mathbf{m}$ is a vector that defines the direction of plastic flow relative to the yield function F.

The following yield function is considered [8]:

$$F(\boldsymbol{\sigma}, \kappa, \bar{\kappa}) = \sigma_e(\boldsymbol{\sigma}) - (1 - \omega(\bar{\kappa}))\,\sigma_y(\kappa) \tag{6}$$

where $\sigma_e(\boldsymbol{\sigma})$ is the Von Mises equivalent stress, κ is the local effective plastic strain measure, $\bar{\kappa}$ is the nonlocal effective plastic strain measure, $\omega \in [0, 1]$ can be interpreted as a nonlocal damage variable, and σ_y is the yield or flow stress. The yield stress can be written as:

$$\sigma_y = \sigma_{y,0} + H\kappa \tag{7}$$

where $\sigma_{y,0}$ is the initial yield strength, and $H > 0$ a hardening modulus. The yield stress is progressively reduced by the factor $(1 - \omega)$ as the damage variable increases from $\omega = 0$ until complete loss of strength, $\omega = 1$. The damage evolution can be described by an exponential relation, a power law, or a linear relation, e.g.,

$$\omega(\bar{\kappa}) = \begin{cases} \frac{\bar{\kappa} - \bar{\kappa}_i}{\bar{\kappa}_u - \bar{\kappa}_i} & \text{if } \bar{\kappa} \leq \bar{\kappa}_u \\ 1 & \text{if } \bar{\kappa} > \bar{\kappa}_u \end{cases} \tag{8}$$

in which $\bar{\kappa}_i$ is the nonlocal effective plastic strain measure at which damage is initiated and $\bar{\kappa}_u$ is the ultimate nonlocal effective plastic strain measure at complete loss of integrity.

The hardening parameter κ is related to the plastic multiplier λ according to the strain-hardening hypothesis:

$$\mathrm{d}\kappa = \sqrt{\frac{2}{3}(\mathrm{d}\boldsymbol{\varepsilon}^p)^{\mathrm{T}}\mathbf{P}\mathrm{d}\boldsymbol{\varepsilon}^p} \tag{9}$$

where, cf. [24],

$$\mathbf{P} = \begin{bmatrix} \frac{2}{3} & -\frac{1}{3} & -\frac{1}{3} & 0 & 0 & 0 \\ -\frac{1}{3} & \frac{2}{3} & -\frac{1}{3} & 0 & 0 & 0 \\ -\frac{1}{3} & -\frac{1}{3} & \frac{2}{3} & 0 & 0 & 0 \\ 0 & 0 & 0 & \frac{1}{2} & 0 & 0 \\ 0 & 0 & 0 & 0 & \frac{1}{2} & 0 \\ 0 & 0 & 0 & 0 & 0 & \frac{1}{2} \end{bmatrix}. \tag{10}$$

Substitution of the flow rule, Equation (5) into the strain-hardening hypothesis, Equation (9), then yields $\mathrm{d}\kappa = \mathrm{d}\lambda$. The yield function F and the plastic multiplier $\mathrm{d}\lambda$ obey the the Karush-Kuhn-Tucker loading-unloading conditions, similar to standard plasticity:

$$\mathrm{d}\lambda \geq 0, \quad F \leq 0, \quad F\mathrm{d}\lambda = 0 \tag{11}$$

The nonlocal effective plastic strain measure, $\bar{\kappa}(\mathbf{x})$, can be defined as the volume average of the local effective plastic strain measure, $\kappa = \kappa(\boldsymbol{\varepsilon}^p)$, as follows:

$$\bar{\kappa}(\mathbf{x}) = \frac{\int_\Omega \phi(\mathbf{x},\mathbf{y})\kappa(\mathbf{y})\mathrm{d}\Omega}{\int_\Omega \phi(\mathbf{x},\mathbf{y})\mathrm{d}\Omega} \tag{12}$$

where $\mathbf{y}$ is the position vector of the infinitesimal volume $\mathrm{d}\Omega$ and ϕ is a weight function. A Gaussian weight function is often assumed:

$$\phi(\mathbf{x},\mathbf{y}) = \frac{1}{(2\pi)^{3/2}\ell^3}\exp\left[-\frac{\|\mathbf{x}-\mathbf{y}\|^2}{2\ell^2}\right] \tag{13}$$

where ℓ is a length scale that sets the averaging volume. The nonlocal formulation in Equation (12) requires the computation of a volume integral at each material point, which is cumbersome and leads to inefficiency. This is usually obviated by using a gradient approximation of the nonlocal model, e.g., [9, 10].

The nonlocal hardening parameter $\bar{\kappa}$ can be approximated when $\kappa(\mathbf{y})$ is expanded in a Taylor series around $\mathbf{x}$,

$$\kappa(\mathbf{y}) = \kappa|_{\mathbf{y}=\mathbf{x}} + \left.\frac{\partial\kappa}{\partial y_i}\right|_{\mathbf{y}=\mathbf{x}}(y_i - x_i) + \frac{1}{2!}\left.\frac{\partial\kappa}{\partial y_i}\right|_{\mathbf{y}=\mathbf{x}}(y_i - x_i)(y_j - x_j) + \mathcal{O}((x_i - y_i)^3) \tag{14}$$

Substitution into Equation (12) and integration in $\mathbb{R}^3$ leads to:

$$\bar{\kappa}(\mathbf{x}) = \kappa(\mathbf{x}) + c_1\nabla^2\kappa(\mathbf{x}) + c_2\nabla^4\kappa(\mathbf{x}) + c_3\nabla^6\kappa(\mathbf{x}) + \cdots \tag{15}$$

in which $\nabla^{2n} = (\nabla^2)^n$ and $\nabla^2 = \sum_i \frac{\partial^2}{\partial x_i^2}$. The coefficients $c_i(\ell)$ depend on the nonlocal averaging function ϕ, and odd derivatives vanish in the integration process due to the isotropic character of ϕ [7, 9]. The nonlocal effective plastic strain measure, $\bar{\kappa}$, can be approximated by truncating the series in Equation (15) after the second-order term. This gradient approximation is known as the *explicit gradient formulation* and it requires $\mathcal{C}^1$-continuous shape functions for the interpolation of κ.

We next take the second-order derivative of Equation (15), multiply by c_1 and substitute the result back into Equation (15). This gives [7]:

$$\bar{\kappa}(\mathbf{x}) - c_1\nabla^2\bar{\kappa}(\mathbf{x}) = \kappa(\mathbf{x}) + (c_2 - c_1^2)\nabla^4\kappa(\mathbf{x}) + (c_3 - c_1c_2)\nabla^6\kappa(\mathbf{x}) + \cdots \tag{16}$$

A formulation requiring only $\mathcal{C}^0$-continuous shape functions is obtained when fourth-order and higher-order terms are omitted in Equation (16) [6, 7]. This implies that coefficients of higher-order terms are set equal to zero, starting with $c_2 - c_1^2 = 0$. It is noted that when Green's weighting function

$$\phi(\mathbf{x},\mathbf{y}) = \frac{1}{4\pi\|\mathbf{x}-\mathbf{y}\|\ell^2}\exp\left[-\frac{\|\mathbf{x}-\mathbf{y}\|}{\ell}\right] \tag{17}$$

$\|\mathbf{x}-\mathbf{y}\|$ being the distance between two points, is substituted for ϕ, no higher-order terms are neglected [10, 8]. The coefficient c_1 then reads:

$$c_1(\ell) = \ell^2. \tag{18}$$

Accordingly, the *second-order implicit gradient formulation* is given by:

$$\bar{\kappa}(\mathbf{x}) - \ell^2\nabla^2\bar{\kappa}(\mathbf{x}) = \kappa(\mathbf{x}) \tag{19}$$

When we include the fourth-order derivatives of Equation (15), multiply by the terms c_i and substitute the result back into Equation (15), the following expression ensues:

$$\bar{\kappa}(\mathbf{x}) - c_1\nabla^2\bar{\kappa}(\mathbf{x}) - (c_2 - c_1^2)\nabla^4\bar{\kappa}(\mathbf{x}) = \kappa(\mathbf{x}) + (c_3 - 2c_1c_2 - c_1^3)\nabla^6\kappa(\mathbf{x}) + \cdots \tag{20}$$

For the Gaussian weight function, $c_1 = \frac{1}{2}\ell^2$, $c_2 = \frac{1}{8}\ell^4$, etc. [25]. When these coefficients are substituted into Equation (20) and sixth-order and higher-order terms are neglected, we obtain the *fourth-order implicit gradient formulation*:

$$\bar{\kappa}(\mathbf{x}) - \frac{1}{2}\ell^2\nabla^2\bar{\kappa}(\mathbf{x}) + \frac{1}{8}\ell^4\nabla^4\bar{\kappa}(\mathbf{x}) = \kappa(\mathbf{x}). \tag{21}$$

For the implicit gradient formulations, the strain-hardening hypothesis is assumed to hold for $\bar{\kappa}$. A state variable $\bar{\lambda}$ is defined as

$$\bar{\lambda}(t) = \max\{\bar{\kappa}(\tau)|0 \leq \tau \leq t\} \tag{22}$$

such that:

$$\mathrm{d}\bar{\lambda} \geq 0, \quad \bar{\kappa} - \bar{\lambda} \leq 0, \quad \mathrm{d}\bar{\lambda}\left[\bar{\kappa} - \bar{\lambda}\right] = 0 \tag{23}$$

Standard static and kinematic boundary conditions are specified on complementary parts of the body surface S:

$$\boldsymbol{\Upsilon}\mathbf{n}_s = \mathbf{t}, \quad \mathbf{u} = \mathbf{u}_s \tag{24}$$

where $\boldsymbol{\Upsilon}$ denotes the stress tensor in matrix form, $\mathbf{n}_s$ is the outward normal to the surface S, and $\mathbf{t}$ is the boundary traction vector. Natural boundary conditions apply on the odd derivatives of $\bar{\kappa}$ [7]:

$$(\mathbf{n}_s^{\mathrm{T}}\nabla)\nabla^n\bar{\kappa} = 0, \quad n = 0, 2 \tag{25}$$

2.2. Weak formulation

The weak form of the governing equations is obtained by setting:

$$\int_V \delta\mathbf{u}^{\mathrm{T}}(\mathbf{L}^{\mathrm{T}}\boldsymbol{\sigma}_{j+1})\mathrm{d}V = \mathbf{0} \tag{26}$$

and

$$\int_V \delta\bar{\lambda}\Big(\bar{\kappa}_{j+1} - c_a\nabla^2\bar{\kappa}_{j+1} + c_b\nabla^4\bar{\kappa}_{j+1} - \kappa_{j+1}\Big)\mathrm{d}V = 0 \tag{27}$$

where δ denotes the variation of a quantity. We obtain the second-order implicit gradient formulation when $c_a = \ell^2$ and $c_b = 0$, while the fourth-order formulation is obtained when $c_a = \frac{1}{2}\ell^2$ and $c_b = \frac{1}{8}\ell^4$. Integrating by parts and applying the divergence theorem yields:

$$\int_V \delta\boldsymbol{\varepsilon}^{\mathrm{T}}\boldsymbol{\sigma}_{j+1}\mathrm{d}V - \int_S \delta\mathbf{u}^{\mathrm{T}}\mathbf{t}_{j+1}\mathrm{d}S = \mathbf{0} \tag{28}$$

and

$$\int_V \Big(\delta\bar{\lambda}\bar{\kappa}_{j+1} - c_a(\nabla\delta\bar{\lambda})^{\mathrm{T}}(\nabla\bar{\kappa}_{j+1}) + c_b\nabla^2\delta\bar{\lambda}\nabla^2\bar{\kappa}_{j+1} - \delta\bar{\lambda}\kappa_{j+1}\Big)\mathrm{d}V = 0 \tag{29}$$

where the boundary condition (25) has been substituted in Equation (29), and the boundary condition for $\mathbf{t}$, Equation $(24)_1$, is applied along the entire external boundary S of the body V.

The following linearisations are carried out at iteration $j+1$ for use in a Newton-Raphson iterative solution procedure:

$$\boldsymbol{\sigma}_{j+1} = \boldsymbol{\sigma}_j + \mathrm{d}\boldsymbol{\sigma}, \quad \kappa_{j+1} = \kappa_j + \mathrm{d}\kappa, \quad \bar{\kappa}_{j+1} = \bar{\kappa}_j + \mathrm{d}\bar{\kappa} \tag{30}$$

where d represents an iterative contribution. Substituting Equation $(30)_1$ into Equations (28) and using (4) gives the weak form:

$$\int_V \delta\boldsymbol{\varepsilon}^{\mathrm{T}}\mathbf{D}^e(\,\mathrm{d}\boldsymbol{\varepsilon} - \mathrm{d}\lambda\mathbf{m})dV = \int_S \delta\mathbf{u}^{\mathrm{T}}\mathbf{t}_{j+1}\mathrm{d}S - \int_V \delta\boldsymbol{\varepsilon}^{\mathrm{T}}\boldsymbol{\sigma}_j\mathrm{d}V \tag{31}$$

Similarly, Equations $(30)_{2,3}$ are substituted into Equation (29) to give

$$\begin{aligned}\int_V \Big(\delta\bar{\lambda}\mathrm{d}\bar{\kappa} - c_a(\nabla\delta\bar{\lambda})^{\mathrm{T}}(\nabla\mathrm{d}\bar{\kappa}) + c_b\nabla^2\delta\bar{\lambda}\nabla^2\mathrm{d}\bar{\kappa} - \delta\bar{\lambda}\mathrm{d}\kappa\Big)\mathrm{d}V = \\ -\int_V \Big(\delta\bar{\lambda}\bar{\kappa}_j - c_a(\nabla\delta\bar{\lambda})^{\mathrm{T}}(\nabla\bar{\kappa}_j) + c_b\nabla^2\delta\bar{\lambda}\nabla^2\bar{\kappa}_j - \delta\bar{\lambda}\kappa_j\Big)\mathrm{d}V\end{aligned} \tag{32}$$

2.3. Stress update

Similar to standard elastoplasticity, the stress update is computed as an integral along a given path from the initial state $(\boldsymbol{\sigma}_0, \boldsymbol{\varepsilon}_0)$ to the final state $(\boldsymbol{\sigma}_{j+1}, \boldsymbol{\varepsilon}_{j+1})$:

$$\boldsymbol{\sigma} = \boldsymbol{\sigma}_0 + \int_{\boldsymbol{\varepsilon}_0}^{\boldsymbol{\varepsilon}_{j+1}} \mathbf{D}^e \mathrm{d}\boldsymbol{\varepsilon} \tag{33}$$

The algorithmic stress update in iteration $j+1$ follows the format [12]:

$$\boldsymbol{\sigma}_{j+1} = \boldsymbol{\sigma}_0 + \mathbf{S}(\boldsymbol{\varepsilon}_0, \boldsymbol{\Delta\varepsilon}_{j+1}) \tag{34}$$

where $\mathbf{S}$ is a non-linear mapping operator and $\boldsymbol{\Delta}$ is the sum of increments in all iterations for the current load step:

$$\boldsymbol{\Delta\varepsilon}_{j+1} = \sum_{i=1}^{j+1} \mathrm{d}\boldsymbol{\varepsilon}_i \tag{35}$$

The yield function is evaluated at every iteration $j+1$ as [8]:

$$F_t = F(\boldsymbol{\sigma}_t, \kappa_0, \bar{\kappa}_{j+1}) = \sigma_{e,t} - \sigma_{y,0}\big(1 - \omega_{j+1}\big) \tag{36}$$

where $(\bullet)_{\bullet,t}$ indicates use of the trial stress which is given by:

$$\boldsymbol{\sigma}_t = \boldsymbol{\sigma}_0 + \mathbf{D}^e \Delta\boldsymbol{\varepsilon}_{j+1}. \tag{37}$$

and $(\bullet)_0$ denotes value at previous converged load step. If $F_t \leq 0$, we have an elastic state and the stress is updated as $\boldsymbol{\sigma}_{j+1} = \boldsymbol{\sigma}_t$. When $F_t > 0$, we have a plastic state which is updated by [17, 3]:

$$\boldsymbol{\sigma}_{j+1} = \boldsymbol{\sigma}_t - \Delta\gamma_{j+1}\mathbf{D}^e\mathbf{m}_t \tag{38}$$

where $\mathbf{m}_t$ is given by Equation $(5)_2$, and $\Delta\gamma_{j+1}$ is the amount of plastic strain for the current iteration, expressed as [8],

$$\Delta\gamma_{j+1} = \frac{F_t}{H\big[1-\omega_{j+1}\big]\big[\frac{\partial\kappa}{\partial\lambda}\big] + \frac{3E}{2(1+\nu)}} \tag{39}$$

in which E is the Young's modulus and ν is the Poisson ratio. This ensures that the consistency condition is satisfied. A concise algorithm is given in the Appendix.

3. DISPERSION ANALYSES

We consider the one-dimensional equation of motion for a bar under uniform tensile loading in rate form:

$$\frac{\partial\dot{\sigma}}{\partial x} = \rho\frac{\partial^2\dot{u}}{\partial t^2} \tag{40}$$

where σ is the stress, ρ is the mass density, u is the displacement, and $(\dot{\bullet})$ denotes the time derivative. The rate of deformation is expressed as

$$\dot{\varepsilon} = \frac{\partial\dot{u}}{\partial x}. \tag{41}$$

An additive decomposition of the strain holds, so that Hooke's law is given by:

$$\dot{\sigma} = E(\dot{\varepsilon} - \dot{\kappa}) \tag{42}$$

The current yield stress has a multiplicative format:

$$\sigma_y = (1 - \omega(\bar{\kappa}))\,(\sigma_{y,0} + H\kappa) \tag{43}$$

while the stress rate $\dot{\sigma}$ has to satisfy the consistency condition: $\dot{F} \equiv \dot{\sigma} - \dot{\sigma}_y = 0$. Differentiating Equation (43) with respect to time yields [20]:

$$\dot{\sigma}_y = \underbrace{(1-\omega)H}_{H_L}\,\dot{\kappa} + \underbrace{\omega'(-\sigma_{y,0} - H\kappa)}_{H_N}\,\dot{\bar{\kappa}} \tag{44}$$

in which $\omega' = \mathrm{d}\omega/\mathrm{d}\bar{\kappa}$, and H_L and H_N can be considered as the current local and nonlocal plastic moduli, respectively. The time derivative of Equation (21) reads:

$$\dot{\bar{\kappa}} - c_a\nabla^2\dot{\bar{\kappa}} + c_b\nabla^4\dot{\bar{\kappa}} = \dot{\kappa}. \tag{45}$$

For a dispersion analysis, we consider the following harmonic functions

$$\dot{u} = \hat{u}\mathrm{e}^{ik(x-ct)}, \quad \dot{\kappa} = \hat{\kappa}\mathrm{e}^{ik(x-ct)}, \quad \dot{\bar{\kappa}} = \hat{\bar{\kappa}}\mathrm{e}^{ik(x-ct)} \tag{46}$$

with k the wave number, c the phase velocity, and the amplitudes $\hat{u}$, $\hat{\kappa}$ and $\hat{\bar{\kappa}}$. The amplitudes $\hat{\kappa}$ and $\hat{\bar{\kappa}}$ can be related by substituting the respective harmonic fields into Equation (45). Using the result together with Equations (41) and (42), the amplitude of the plastic strain, $\hat{\kappa}$, can be related to $\hat{u}$, the amplitude of the displacement. Subsequently, satisfaction of the consistency condition can be exploited to equal the right-hand sides of Equations (42) and (44). The resulting expression reads:

$$Ek^2\left[\frac{H_L(1 + c_ak^2 + c_bk^4) + H_N}{(H_L + E)(1 + c_ak^2 + c_bk^4) + H_N}\right] = \rho k^2c^2 \tag{47}$$

Using the bar velocity, $c_e = \sqrt{E/\rho}$, the phase velocity c can be expressed as:

$$\frac{c^2}{c_e^2} = \left[\frac{H_L(1 + c_ak^2 + c_bk^4) + H_N}{(H_L + E)(1 + c_ak^2 + c_bk^4) + H_N}\right]. \tag{48}$$

The normalised wave velocity c/c_e is plotted as a function of the normalised wave number $k\ell$ in Figure 1 for $H_L = 1819\ \mathrm{N/mm^2}$, $H_N = -2148\ \mathrm{N/mm^2}$, $E = 20000\ \mathrm{N/mm^2}$ and $\ell = 1.0\ \mathrm{mm}$, being representative values for a low-strength concrete. For comparison, the dispersion relation for the explicit gradient plasticity model [15],

$$\frac{c^2}{c_e^2} = \left[\frac{H_E + gk^2}{E + H_E + gk^2}\right] \tag{49}$$

has been plotted in the same figure for a softening modulus $H_E = -329\ \mathrm{N/mm^2}$ and $g = -\ell^2H_E$. The frequency $\omega = kc$ is a function of wave number, $\omega = \omega(k)$. Since $\omega''(k) \neq 0$, wave propagation is dispersive [15, 26].

The critical wave number k_{crit} is the minimum wave number below which only imaginary values of phase velocity exist. It is obtained by setting the phase velocity $c = 0$. The critical wave length $\mu_{crit} = 2\pi/k_{crit}$ is the wave length above which no waves will propagate:

$$\begin{aligned}
&\text{second-order implicit formulation} \quad \mu_{crit} = 2\pi\ell\sqrt{-\frac{(H_N + H_L)}{H_L}} \\
&\text{fourth-order implicit formulation} \quad \mu_{crit} = 2\pi\ell\sqrt{-2 + 2\sqrt{\frac{-(H_L + 2H_N)}{H_L}}} \\
&\text{second-order explicit formulation} \quad \mu_{crit} = 2\pi\ell
\end{aligned} \tag{50}$$

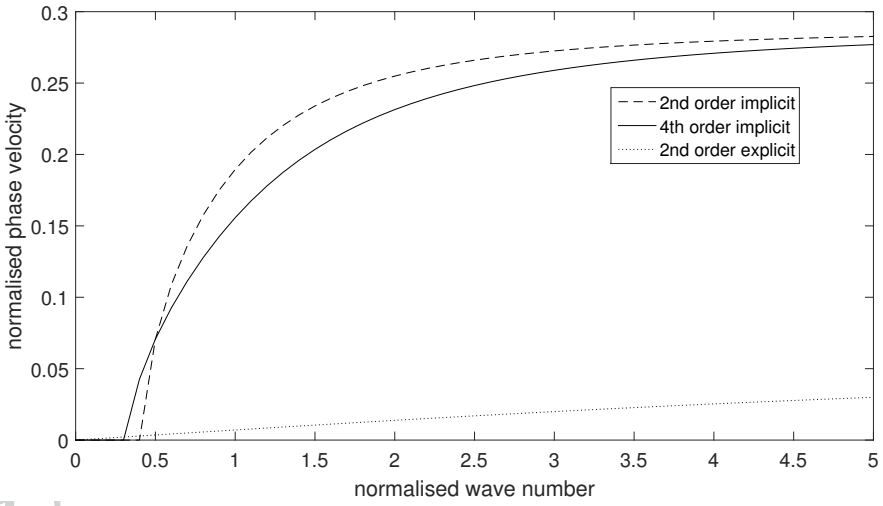

Figure 1. Normalised phase velocity c/c_e as a function of normalised wave number $k\ell$.

We now proceed by using the linear damage relation of Equation (8) and use this to derive the expressions for the local and nonlocal hardening moduli for the implicit gradient plasticity formulation:

$$H_L = \begin{cases} H\left(1 - \frac{\bar{\kappa}-\bar{\kappa}_i}{\bar{\kappa}_u-\bar{\kappa}_i}\right) & \text{if } \bar{\kappa} \leq \bar{\kappa}_u \\ 0 & \text{if } \bar{\kappa} > \bar{\kappa}_u \end{cases} \tag{51}$$

and

$$H_N = \begin{cases} -(\sigma_{y,0} + H\kappa)\left(\frac{1}{\bar{\kappa}_u-\bar{\kappa}_i}\right) & \text{if } \bar{\kappa} \leq \bar{\kappa}_u \\ 0 & \text{if } \bar{\kappa} > \bar{\kappa}_u \end{cases} \tag{52}$$

The normalised critical wave length μ_{crit}/ℓ is plotted *vs* the strain level $\kappa = \bar{\kappa}$ in Figure 2 for $\bar{\kappa}_i = 0$, $\bar{\kappa}_u = 0.001$, $H = 2000\ \mathrm{N/mm^2}$ and $\sigma_{y,0} = 2\ \mathrm{N/mm^2}$. For the explicit gradient plasticity formulation, the critical wavelength is non-zero and independent of the accumulated damage, so that there is localisation into a non-zero band width. For the implicit gradient plasticity formulations, a non-zero band width results, except when the damage attains a maximum, when the localisation width becomes zero. It has been argued that this can be conceived as an an advantage of implicit gradient plasticity formulations, since they ultimately result in a sharp crack [8]. Conversely, it can be considered as a disadvantage, as in the limiting case of a sharp crack, the topology changes and boundary conditions have to be supplied locally in order to keep the boundary value problem well-posed.

Indeed, the critical wave length represents the width of the localisation band. It is clear from Figure 2 that, at the initial stages of the deformation, the second-order implicit formulation has a localisation band that is wider than that which results from the fourth-order implicit formulation. However, at some point, before complete failure, the localisation band width of the fourth-order formulation becomes higher, and remains so.

When using an exponential damage law [8], for instance

$$\omega = 1 - \mathrm{e}^{-\beta\bar{\kappa}} \tag{53}$$

the results become different, see Figure 3 for $\beta = 1000$. Now, neither the explicit formulation, nor either of the implicit gradient plasticity formulutions result in a zero critical wave length at complete damage, and thus, convergence to a line crack does not take place in either of the cases which have been considered. As a minor detail we note that the band width of the second-order gradient plasticity model remains wider than that of the fourth-order model for all strain levels.

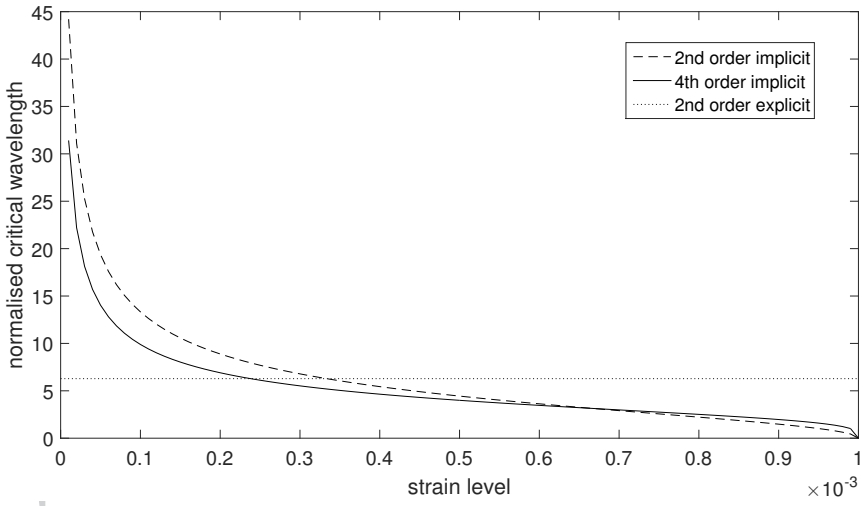

Figure 2. Normalised critical wavelength μ_{crit}/ℓ *vs* the strain level $\kappa = \bar{\kappa}$ for a piece-wise linear damage law.

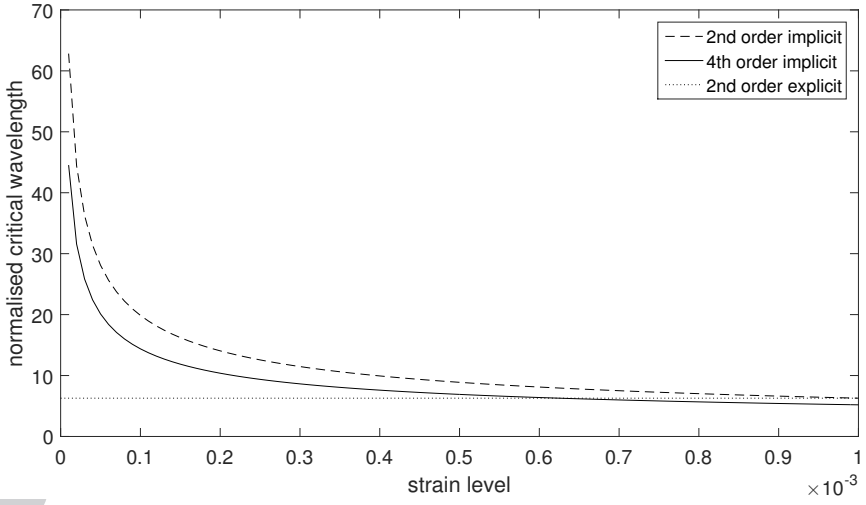

Figure 3. Normalised critical wavelength μ_{crit}/ℓ *vs* the strain level $\kappa = \bar{\kappa}$ for an exponential damage law.

The relations for the critical wave length, Equations (50), indicate that the sum of the local and nonlocal hardening moduli, H_L and H_N determine whether or not regularisation is achieved for the implicit gradient formulations. For the second-order implicit gradient plasticity formulation, $H_L + H_N$ has to be negative. According to the adopted yield function, Equation (43), H_L is always positive and H_N is always negative because $H > 0$. The sum of the two moduli is initially positive but at a certain loading stage, it becomes negative. The same holds for the fourth-order implicit gradient plasticity formulation, except that now the sum under consideration is $H_L + 2H_N$. For the second-order explicit formulation, $H_E < 0$, and regularisation is always achieved.

The behaviour of localised zones in softening systems depends on the dispersive properties of the material [27, 28]. At wave lengths below μ_{crit}, waves with real phase velocities exhibit dispersion. Hence, the localisation zone can extend, and the strain profile in the localisation zone can be transformed due to different modes travelling at different speeds. In the static case, phase velocity

$c = 0$, the localisation zone acts as a stationary wave and the width of the localisation zone is equal to the lowest-order wave that the system can transmit [15, 27].

4. ISOGEOMETRIC FINITE ELEMENT DISCRETISATION

4.1. NURBS-based Bézier element

We use NURBS functions to describe the geometry as well as for analysis. A univariate NURBS is expressed as:

$$R_{a,p}(\xi) = \frac{w_a B_{a,p}(\xi)}{\mathbf{W}(\xi)} \tag{54}$$

where $B_{a,p}(\xi)$ is a B-spline function, w_a is the NURBS weight and

$$\mathbf{W}(\xi) = \sum_{b=1}^{n} w_b B_{b,p}(\xi) \tag{55}$$

represents the weight function. For a polynomial of degree $p = 0$, the B-spline function is defined as:

$$B_{a,0}(\xi) = \begin{cases} 1, & \xi_a \leq \xi \leq \xi_{a+1} \\ 0, & \text{otherwise} \end{cases} \tag{56}$$

for a parametric coordinate, or knot, ξ [22]. For $p > 0$, B-spline functions are defined by the Cox-de Boor recursion formula [29, 30],

$$B_{a,p}(\xi) = \frac{\xi - \xi_a}{\xi_{a+p} - \xi_a} B_{a,p-1}(\xi) + \frac{\xi_{a+p+1} - \xi}{\xi_{a+p+1} - \xi_{a+1}} B_{a+1,p-1}(\xi) \tag{57}$$

Multivariate NURBS shape functions are obtained as tensor products of the univariate shape functions.

Different from Lagrange shape functions, NURBS shape functions are not local to an element. In order to make NURBS shape functions suitable for analysis in the standard finite element format, we employ Bézier extraction [23]. The Bézier representation for a one-dimensional element e is expressed as:

$$\mathbf{R}^e(\xi) = \mathbf{W}^e \mathbf{C}^e \frac{\mathbf{G}^e(\xi)}{W^e(\xi)} \tag{58}$$

with

$$W^e(\xi) = (\mathbf{w}^e)^{\mathrm{T}} \mathbf{C}^e \mathbf{G}^e(\xi) \tag{59}$$

where $\mathbf{R}$ contains the NURBS basis functions, $\mathbf{C}$ is the Bézier extraction operator, $\mathbf{w}$ is a vector of the NURBS weights, and $\mathbf{G}$ contains the Bézier basis functions (Bernstein polynomials).

4.2. Orders of interpolation

The displacement field, $\mathbf{u}$, and the nonlocal effective plastic strain measure (nonlocal plastic multiplier), $\bar{\lambda}$, are discretised as follows:

$$\mathbf{u} = \mathbf{N}\mathbf{a} \tag{60}$$

and

$$\bar{\lambda} = \mathbf{h}^{\mathrm{T}} \bar{\mathbf{\Lambda}} \tag{61}$$

where $\mathbf{a}$ is a vector of discrete displacements at the control points, $\bar{\mathbf{\Lambda}}$ is a vector of the nonlocal plastic multiplier degrees of freedom at the control point, $\mathbf{N}$ is a matrix, and $\mathbf{h}$, a vector, both containing NURBS shape functions. Based on the linear kinematic relation (3), the strain vector can

be expressed as:

$$\boldsymbol{\varepsilon} = \mathbf{B}\mathbf{a} \tag{62}$$

where $\mathbf{B} = \mathbf{L}\mathbf{N}$. In a similar way, the gradient of the nonlocal plastic multiplier $\nabla\bar{\lambda}$ and its Laplacian can be discretised as:

$$\nabla\bar{\lambda} = \mathbf{Q}^{\mathrm{T}}\bar{\mathbf{\Lambda}} \tag{63}$$

$$\nabla^2\bar{\lambda} = \mathbf{p}^{\mathrm{T}}\bar{\mathbf{\Lambda}} \tag{64}$$

where

$$\mathbf{Q} = [\nabla h_1, \nabla h_2, \ldots, \nabla h_{ns}]^{\mathrm{T}} \tag{65}$$

$$\mathbf{p} = [\nabla^2 h_1, \nabla^2 h_2, \ldots, \nabla^2 h_{ns}]^{\mathrm{T}} \tag{66}$$

and ns the number of shape functions at each control point. The interpolation functions contained in $\mathbf{h}$ must be C^0-continuous and C^1-continuous for the second-order and fourth-order formulations, respectively. Quadratic NURBS are used for $\mathbf{h}$, and since the strain vector (which is of the same order as the nonlocal plastic multiplier) is one order lower than the displacement, cubic NURBS are used for $\mathbf{N}$. This is investigated further in Section 5.

To construct conforming meshes of different orders and matching element boundaries, we use Bézier projection [31]:

$$\mathbf{P}^{e,p'} = (\mathbf{R}^{e,p'})^{\mathrm{T}}(\mathbf{E}^{p,p'})^{\mathrm{T}}(\mathbf{C}^{e,p})^{\mathrm{T}}(\mathbf{P}^{e,p}) \tag{67}$$

where $\mathbf{P}^{e,p}$ contains the control points of the initial curve of order p, $\mathbf{P}^{e,p'}$ contains the control points of the target curve of order p', $\mathbf{C}^{e,p}$ contains the initial Bézier extraction operator, $\mathbf{R}^{e,p'}$ is the inverse of the target Bézier extraction operator, i.e. $\mathbf{R}^{e,p'} = (\mathbf{C}^{e,p'})^{-1}$, and $\mathbf{E}^{p,p'}$ is the elevation matrix from degree p to p'. It is noted that the Bézier extraction/projection procedure preserves the original continuity.

4.3. Spatial discretisation

The interpolation functions of Equations (60)–(61) are used to discretise the weak forms, Equations (31) and (32). Requiring that the result must hold for all admissible $\delta\mathbf{a}$ and $\delta\mathbf{\Lambda}$ leads to the following set of non-linear algebraic equations [8]:

$$\begin{bmatrix} \mathbf{K}_{aa} & \mathbf{K}_{a\lambda} \\ \mathbf{K}_{\lambda a} & \mathbf{K}_{\lambda\lambda} \end{bmatrix} \begin{bmatrix} \mathrm{d}\mathbf{a} \\ \mathrm{d}\bar{\mathbf{\Lambda}} \end{bmatrix} = \begin{bmatrix} \mathbf{f}_e - \mathbf{f}_a \\ -\mathbf{f}_\lambda \end{bmatrix} \tag{68}$$

with the elastic stiffness matrix

$$\mathbf{K}_{aa} = \int_V \mathbf{B}^{\mathrm{T}}\mathbf{A}_{aa}\mathbf{B}\mathrm{d}V, \tag{69}$$

the off-diagonal matrices

$$\mathbf{K}_{a\lambda} = -\int_V \mathbf{B}^{\mathrm{T}}\mathbf{A}_{a\lambda}\mathbf{h}\,\mathrm{d}V, \quad \mathbf{K}_{\lambda a} = -\int_V \mathbf{h}^{\mathrm{T}}\mathbf{A}_{\lambda a}\mathbf{B}\,\mathrm{d}V, \tag{70}$$

the gradient-dependent matrix

$$\mathbf{K}_{\lambda\lambda} = \int_V \mathbf{h}^{\mathrm{T}}\big(1 - A_{\lambda\lambda}\big)\mathbf{h} + c_a\mathbf{Q}^{\mathrm{T}}\mathbf{Q} + c_b\mathbf{p}^{\mathrm{T}}\mathbf{p}\,\mathrm{d}V, \tag{71}$$

the external force vector

$$\mathbf{f}_e = \int_S \mathbf{N}^{\mathrm{T}}\mathbf{t}_{j+1}\mathrm{d}S, \tag{72}$$

the vector of control point forces (equivalent to internal stresses)

$$\mathbf{f}_a = -\int_V \mathbf{B}^{\mathrm{T}}\boldsymbol{\sigma}_j\mathrm{d}V, \tag{73}$$

and the vector associated with the nonlocal averaging

$$\mathbf{f}_\lambda = \mathbf{K}_\lambda \bar{\lambda}_j - \int_V \mathbf{h}^{\mathrm{T}} \lambda_j \, \mathrm{d}V \tag{74}$$

where

$$\mathbf{K}_\lambda = \int_V \mathbf{h}^{\mathrm{T}}\mathbf{h} + c_a \mathbf{Q}^{\mathrm{T}}\mathbf{Q} + c_b \mathbf{p}^{\mathrm{T}}\mathbf{p} \, \mathrm{d}V. \tag{75}$$

The arrays $\mathbf{A}_{aa}$, $\mathbf{A}_{a\lambda}$ and $\mathbf{A}_{\lambda a}$, and the scalar $\mathbf{A}_{\lambda\lambda}$ are defined as [8, 17]:

$$\mathbf{A}_{aa} = \mathbf{A} - \frac{\mathbf{A}\mathbf{m}\mathbf{m}^{\mathrm{T}}\mathbf{A}}{H\big(1-\omega\big)\big(\frac{\partial \kappa}{\partial \lambda}\big) + \frac{3E}{2(1+\nu)}} \tag{76}$$

$$\mathbf{A}_{a\lambda} = \frac{\sigma_y\big(\frac{\partial \omega}{\partial \bar{\kappa}}\big)\big(\frac{\partial \bar{\kappa}}{\partial \lambda}\big)\mathbf{A}\mathbf{m}}{H\big(1-\omega\big)\big(\frac{\partial \kappa}{\partial \lambda}\big) + \frac{3E}{2(1+\nu)}} \tag{77}$$

$$\mathbf{A}_{\lambda a} = \frac{\mathbf{m}^{\mathrm{T}}\mathbf{A}}{H\big(1-\omega\big)\big(\frac{\partial \kappa}{\partial \lambda}\big) + \frac{3E}{2(1+\nu)}} \tag{78}$$

$$A_{\lambda\lambda} = \frac{\sigma_y\big(\frac{\partial \omega}{\partial \bar{\kappa}}\big)\big(\frac{\partial \bar{\kappa}}{\partial \lambda}\big)}{H\big(1-\omega\big)\big(\frac{\partial \kappa}{\partial \lambda}\big) + \frac{3E}{2(1+\nu)}} \tag{79}$$

respectively, where $\mathbf{A}$ is the algorithmic stiffness operator

$$\mathbf{A} = \left[(\mathbf{D}^e)^{-1} + \Delta\gamma \frac{\partial \mathbf{m}}{\partial \boldsymbol{\sigma}}\right]^{-1} \tag{80}$$

5. INTERPOLATION REQUIREMENTS

Taking the order of interpolation for the nonlocal effective plastic strain measure to be an order lower than the displacement gives a balanced interpolation. It is useful to investigate the effect of the same orders of interpolation, because when using adaptive or hierarchical refinement, the same order of interpolation may be simpler to implement. Indeed, it has been argued that nonlocal gradient models are coupled problems and the interpolation orders of variables do not have to be balanced [32]. Finally, there are indications from calculations with the second-order explicit gradient plasticity model that stress oscillations can occur in spite of the use of different interpolation orders for the displacements and the plastic multiplier [13].

We consider a one-dimensional bar, which is fixed at one end and subjected to tension at the other end, see Figure 4. The bar has a length $L = 100$ mm, a Young's modulus $E = 20000\ \mathrm{N/mm^2}$, area $= 100\ \mathrm{mm^2}$ and an initial tensile strength $\sigma_{y,0} = 2\ \mathrm{N/mm^2}$. The tensile strength in the central part of the bar (21.875mm) is reduced by 5% to trigger localisation. A length scale $\ell = 5$ mm is used and the bar is discretised with 64 and 128 elements, respectively. Only the second-order implicit gradient plasticity formulation is considered in this section.

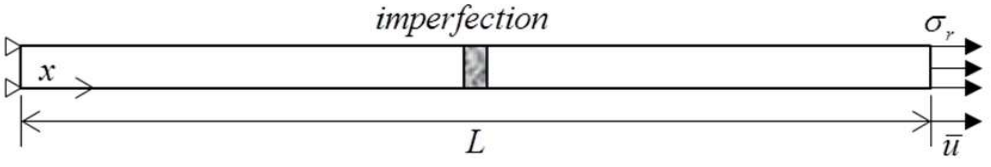

Figure 4. Tensile bar with imperfection

First, the effect of material parameters is studied for the tensile bar without imperfection. The load displacement curves are given in Figure 5 considering a linear damage evolution, Equation

(8), with $H = 6000\ \mathrm{N/mm^2}$ and $\bar{\kappa}_i = 0$, and for an exponential damage evolution, Equation (53), with $H = 6000\ \mathrm{N/mm^2}$. The critical nonlocal effective plastic strain at full damage $\bar{\kappa}_u$ shows a significant influence on the linear relation, while β is the dominating parameter when using the exponential relation, cf. [8].

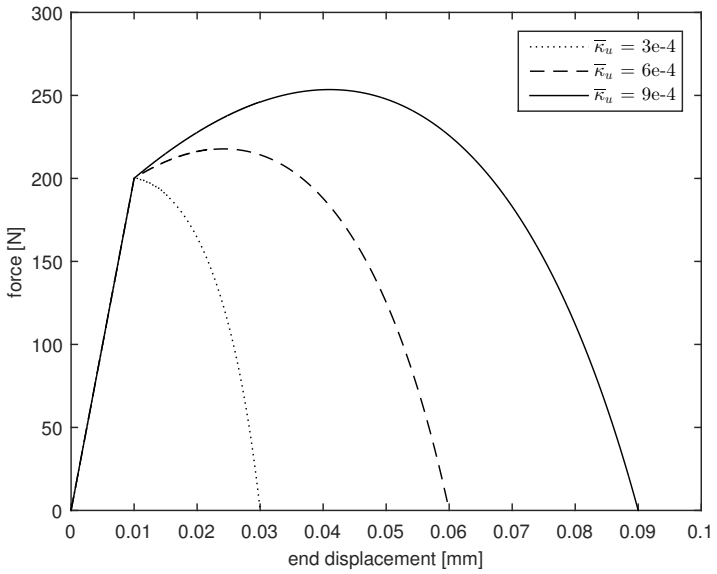

(a)

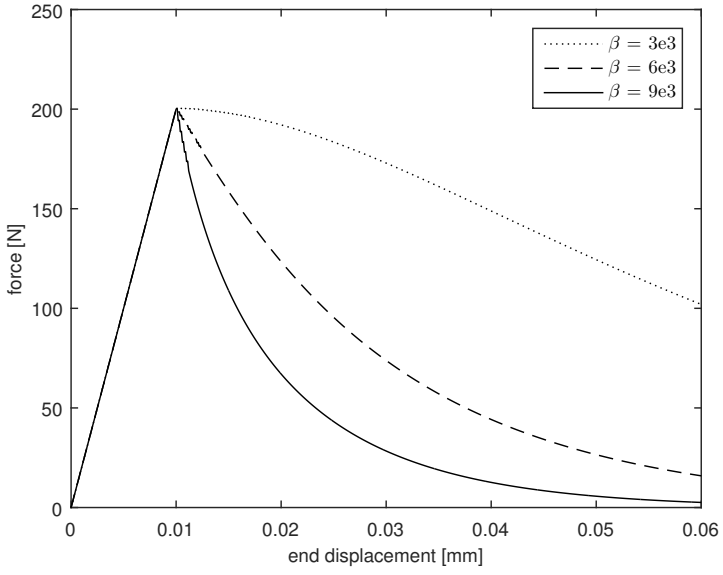

(b)

Figure 5. Influence of material parameters for bar without imperfection discretised with 64 elements using linear (a) and exponential (b) damage evolution law. Results are shown for an interpolation order $p = 2$ of the nonlocal plastic multiplier and $p = 3$ of the displacement.

All subsequent simulations are for the tensile bar with an imperfection. The load-displacement curves are shown in Figure 6 for a quadratic interpolation of the nonlocal plastic multiplier and a cubic interpolation of the displacement. The parameters $H = 2000\ \mathrm{N/mm^2}$, $\bar{\kappa}_i = 0$ and $\bar{\kappa}_u = 0.001$

are used for linear damage evolution, while $H = 9000\ \mathrm{N/mm^2}$ and $\beta = 4300$ are adopted for exponential damage evolution. It is clear that mesh-objective results are obtained, since the curves are identical for both discretisations (64 and 128 elements). The evolution of nonlocal effective plastic strain has been plotted in Figure 7. The load-displacement curves as well as the nonlocal effective plastic strain profiles converge throughout the loading history. No visible mesh dependency exists.

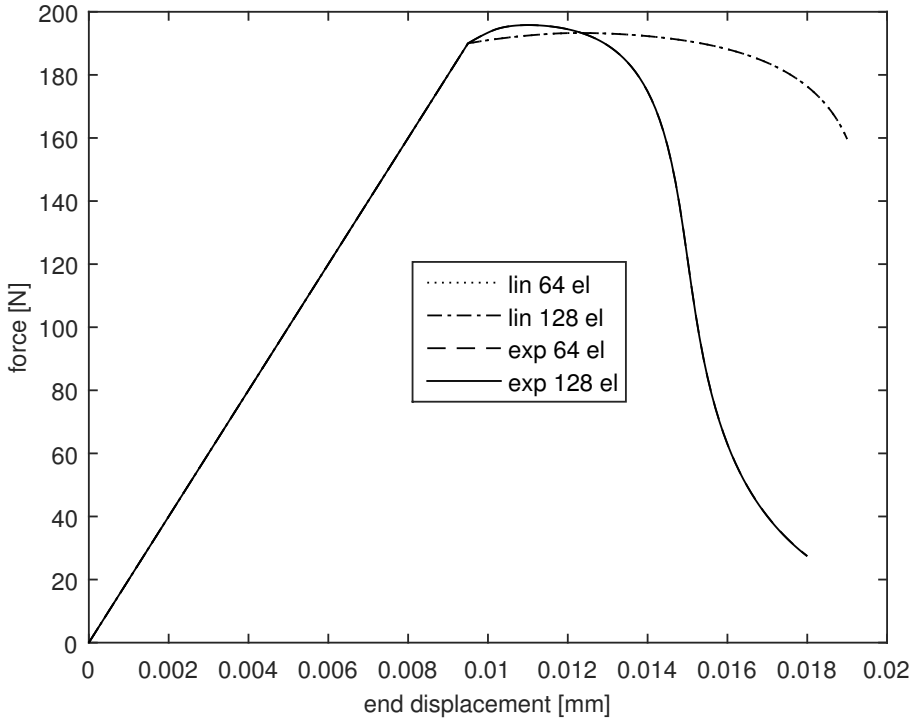

Figure 6. Load-displacement curves using an interpolation order $p = 2$ for the nonlocal plastic multiplier and $p = 3$ for the displacements. Results are shown for linear and exponential damage evolution relations, with 64 and 128 elements.

Next, we consider the same interpolation order for the displacements and for the nonlocal effective plastic strain, using an exponential damage evolution. The load-displacement curves as well as the nonlocal strain profiles converge upon refinement of the discretisation. For 128 elements, the results are compared in Figure 8 for quadratic/quadratic, cubic/cubic and cubic/quadratic interpolations. There seems to be no visible differences among the results. The axial stress and the yield stresses are shown in Figures 9 and again, there seems to be no significant differences, which supports the assertion that gradient formulations are coupled problems and the interpolation functions of different variables that have to be discretised are not necessarily related [32]. Oscillations in the axial stress persist for all interpolations, which is ascribed to the weak satisfaction of the yield condition, similar to results obtained for the second-order explicit gradient plasticity model [13].

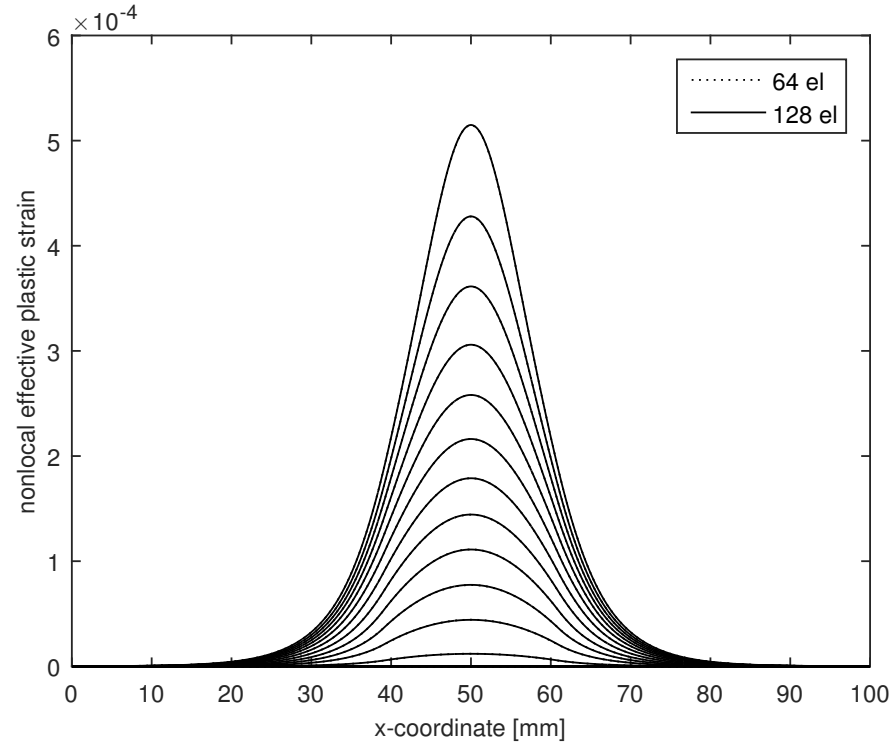

(a)

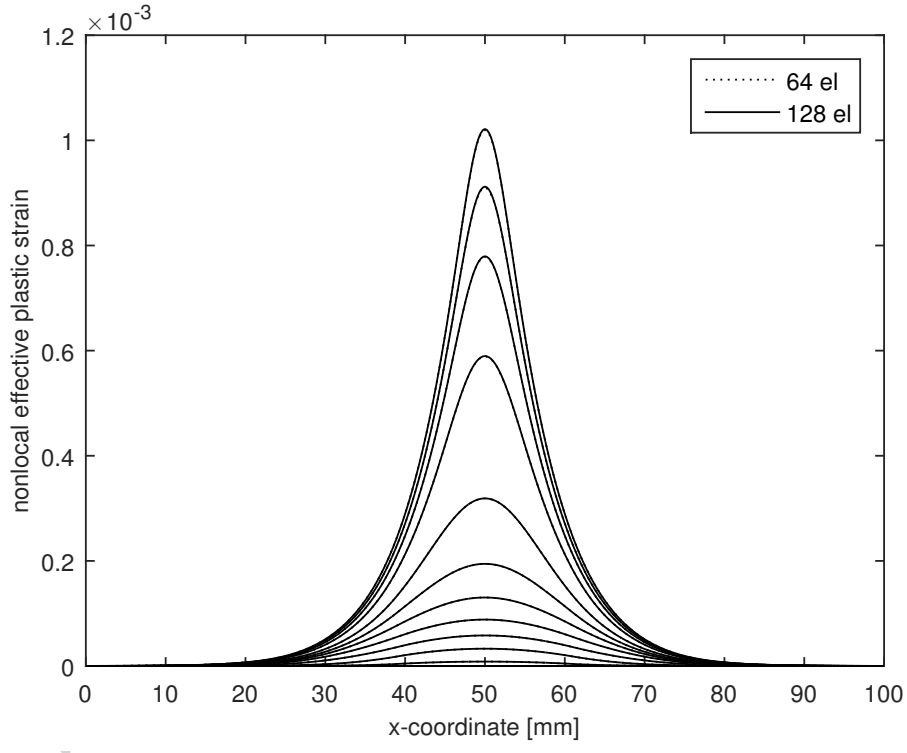

(b)

Figure 7. Evolution of the nonlocal effective plastic strain for linear (a) and exponential (b) damage evolution law with 64 and 128 elements. Results are shown for an interpolation order $p = 2$ of the nonlocal plastic multiplier and $p = 3$ of the displacement.

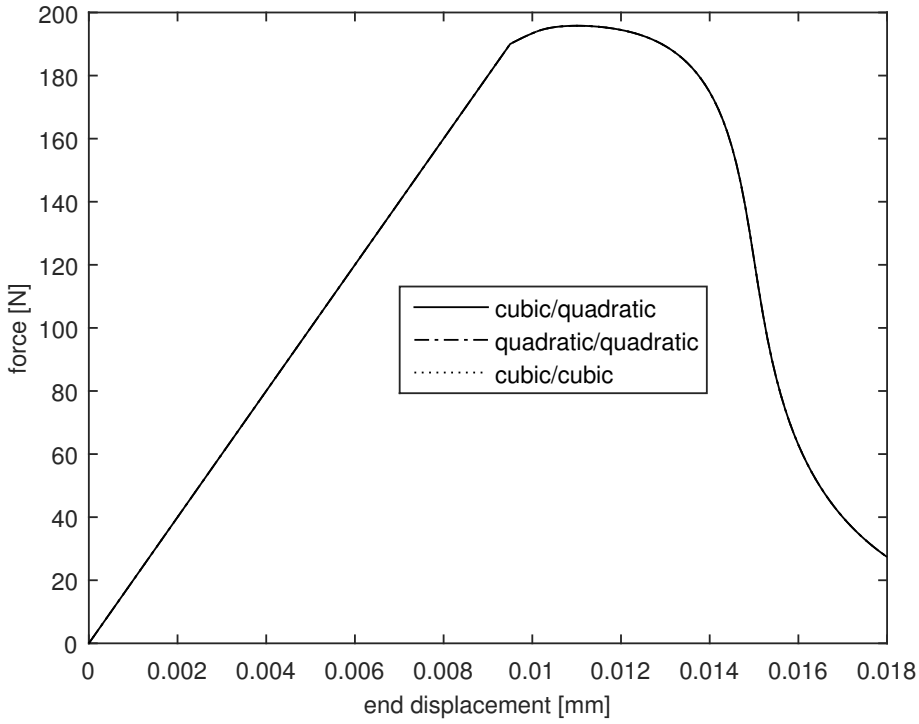

(a)

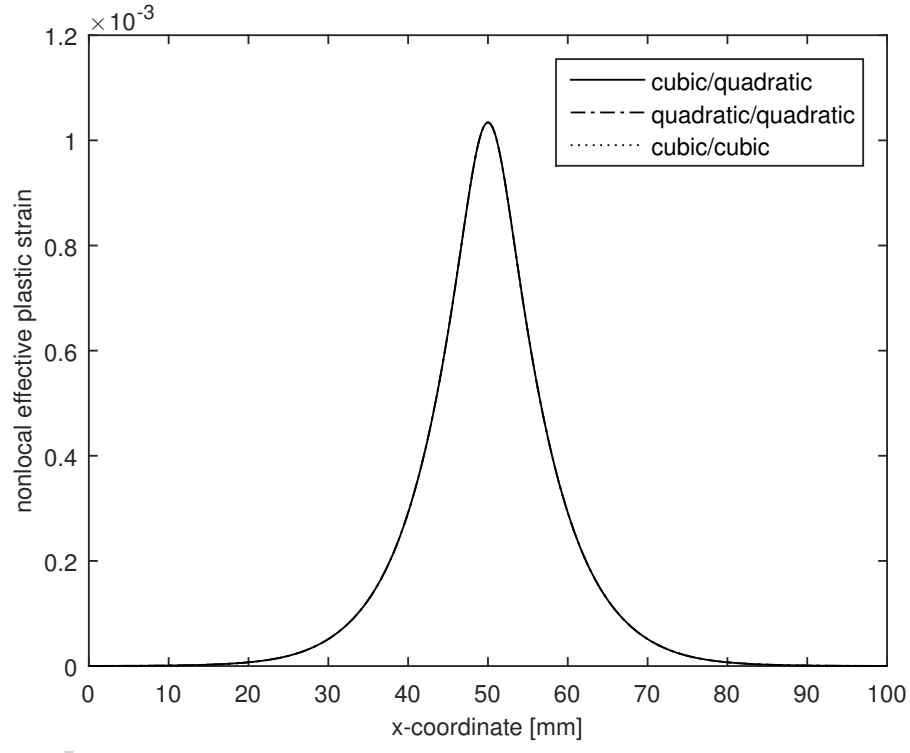

(b)

Figure 8. Load-displacement curves (a) and nonlocal effective plastic strain profiles (b) for different and same interpolation orders for the displacement/nonlocal effective plastic strain. Discretisation with 128 elements and an exponential damage evolution is adopted.

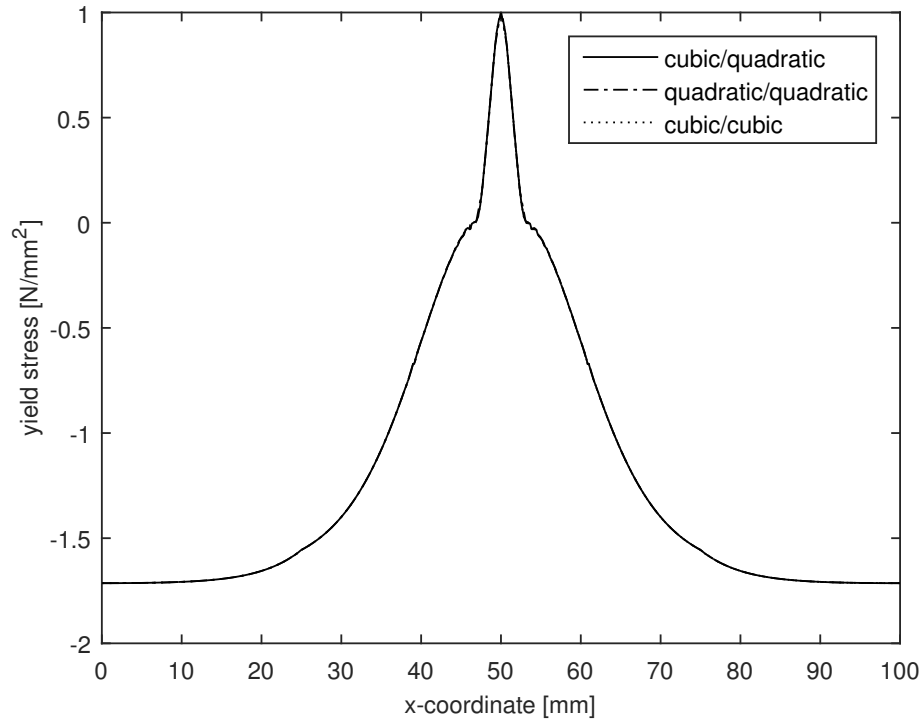

(a)

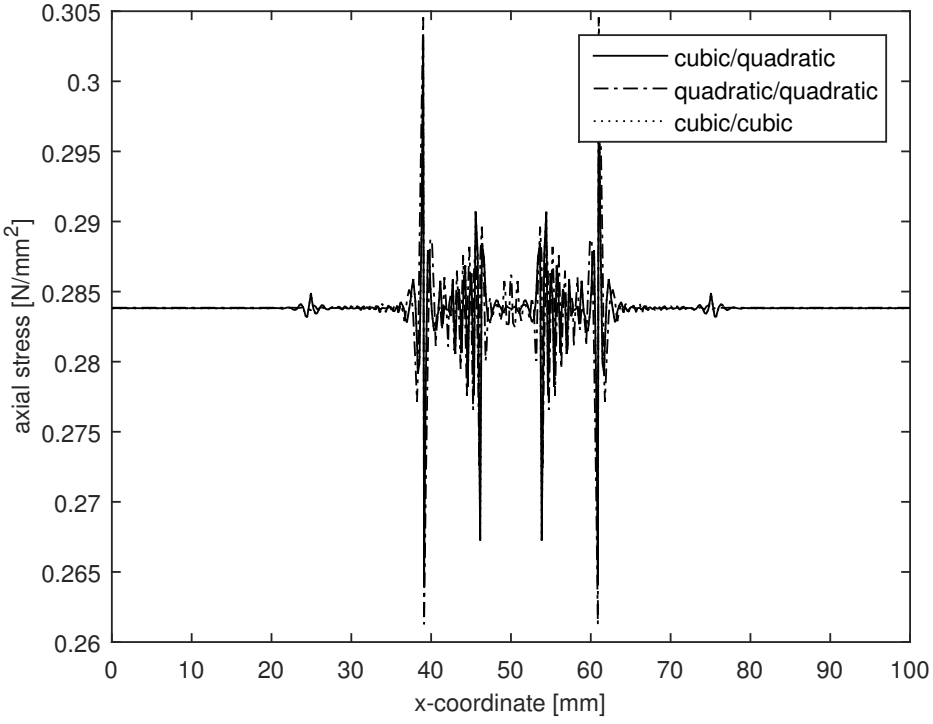

(b)

Figure 9. Yield stress (a) and axial stress (b) for different and same interpolation orders for the displacement/nonlocal effective plastic strain. Discretisation is with 128 elements and a exponential damage evolution is adopted.

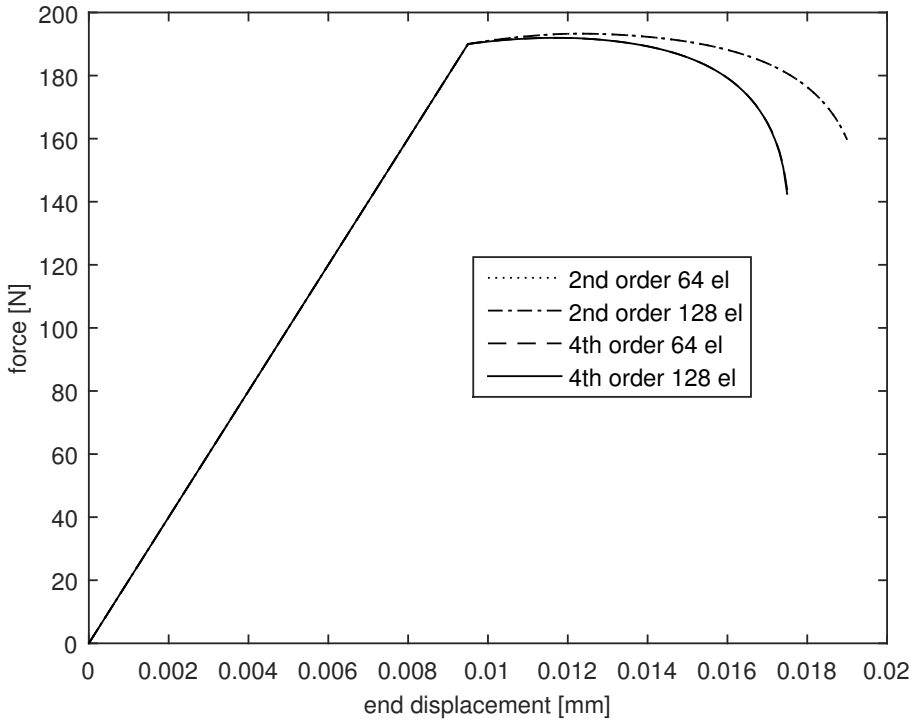

(a)

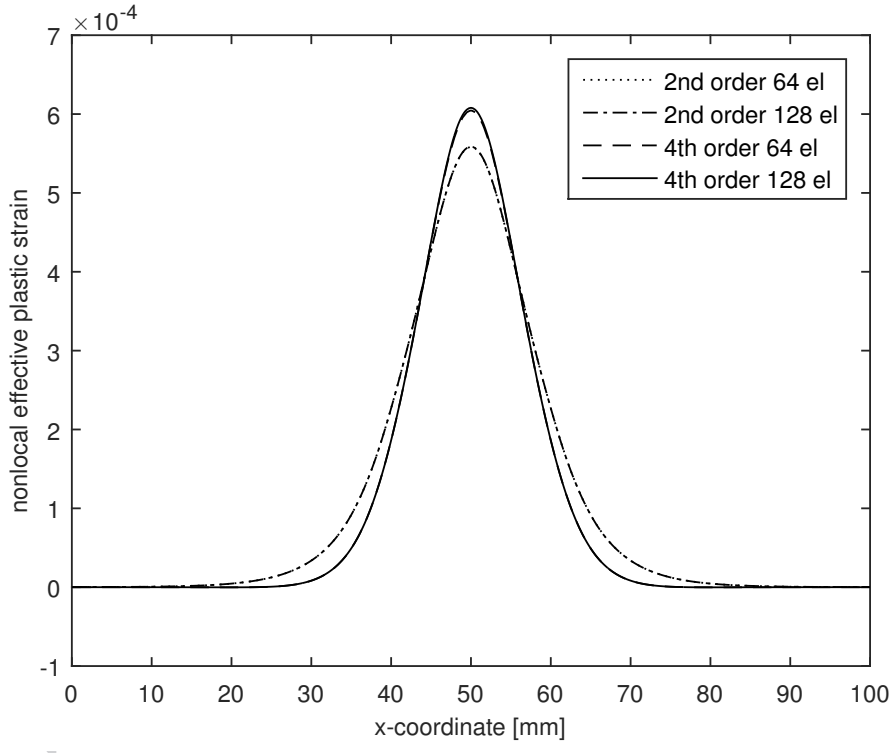

(b)

Figure 10. Tensile bar: Load-displacement curves (a) and nonlocal effective plastic strain profiles (b) for the second-order and fourth-order formulations discretised with different number of elements.

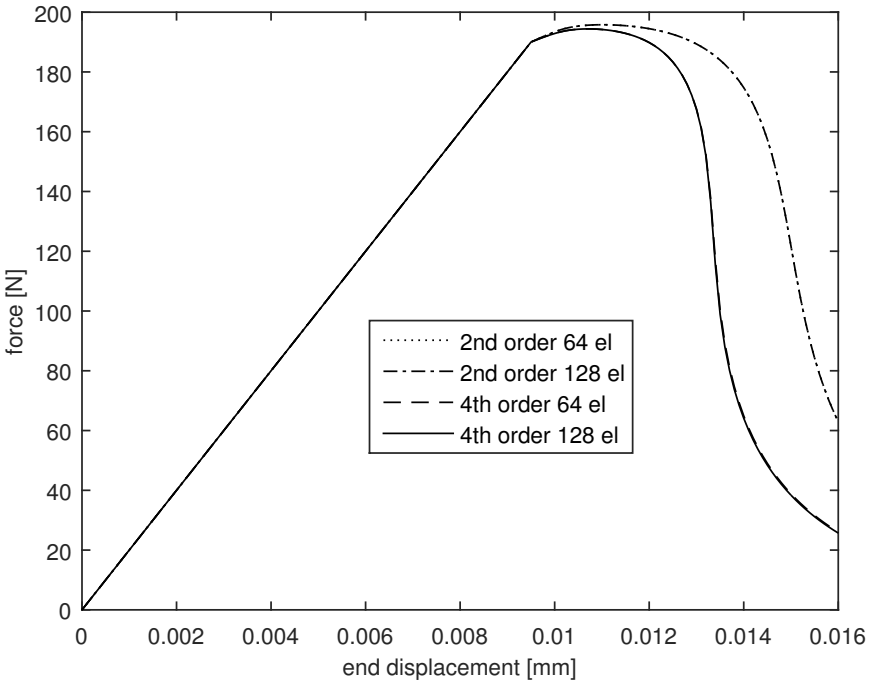

(a)

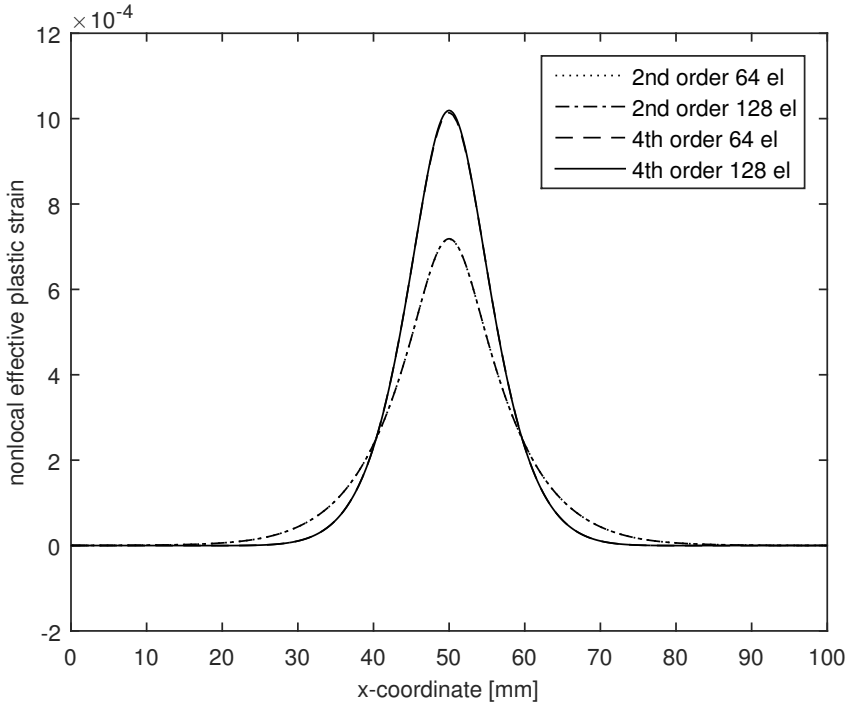

(b)

Figure 11. Tensile bar: Load-displacement curves (a) and nonlocal effective plastic strain profiles (b) for second-order and fourth-order gradient formulations discretised with different number of elements. An exponential damage evolution relation is adopted.

6. COMPARISON OF SECOND-ORDER AND FOURTH-ORDER GRADIENT FORMULATIONS

6.1. One-dimensional bar in tension

We revisit the problem of an imperfect bar subjected to tension discussed in the previous section (Figure 4). We now consider the second-order and the fourth-order implicit gradient plasticity formulations using a cubic interpolation for the displacements and a quadratic interpolation for the nonlocal effective plastic strain. We recall that for the second-order gradient formulation, $c_a = \ell^2$, $c_b = 0$, and that for the fourth-order formulation $c_a = \ell^2/2$, $c_b = \ell^4/8$. The load-displacement curves and nonlocal effective plastic strain profiles are shown in Figure 10 for a linear damage evolution.

Convergence is achieved in all cases, but significant differences occur between both formulations. The second-order implicit gradient formulation shows a more ductile response and a broader localisation band than the fourth-order formulation. This supports the results of the dispersion analysis, Figure 2, which point at a broader localisation band for the second-order formulation. The additional term due to the non-zero coefficient c_b in the fourth-order formulation leads to a higher peak of the nonlocal effective plastic strain in the fourth-order formulation, see Figure 10(b). The same trend is observed for the exponential damage evolution law, see Figure 11.

6.2. Square plate under uniaxial tension

Next, the two-dimensional panel is considered shown in Figure 12. The left side is fixed in the x direction and the midpoint of this side is fixed in the y direction as well. A displacement $\bar{u}$ is imposed on the right side. Regarding the panel dimensions $L = 10$ mm, and the material properties are $E = 20000\ \mathrm{N/mm^2}$, $H = 2000\ \mathrm{N/mm^2}$, and $\sigma_{y,0} = 2\ \mathrm{N/mm^2}$. An exponential damage evolution is assumed with $\beta = 3500$ and a length scale $\ell = 0.7$ mm. The yield strength is reduced by 5% at the bottom left corner of the panel to trigger localisation. Three uniformly refined meshes are considered with 256, 1,024 and 4,096 elements, respectively, see Figure 13, with a cubic interpolation for the displacements and a quadratic interpolation for the pressure.

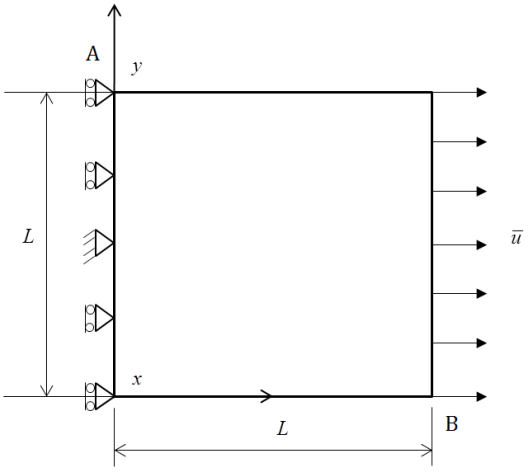

Figure 12. Geometry and boundary conditions of two-dimensional panel subjected to uniaxial tension

The load-displacement curves are shown in Figure 14 for different meshes. The results show no mesh dependency indicating that regularisation is achieved. The contours of the nonlocal effective plastic strain are given in Figure 15, while Figure 16 shows its distribution along the diagonal AB (Figure 12). The second-order formulation shows a wider localisation band. This is similar to the findings for implicit second-order and fourth-order gradient damage formulations [7].

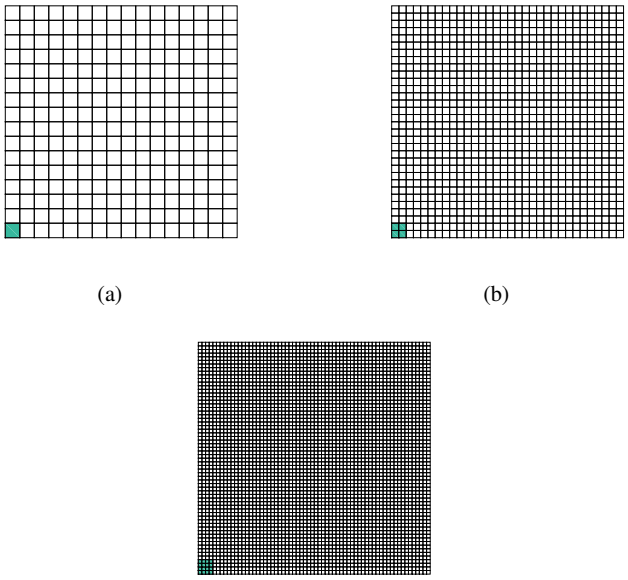

Figure 13. Meshes of square panel indicating weakened elements: (a) 256 elements; (b) 1,024 elements; (c) 4,096 elements

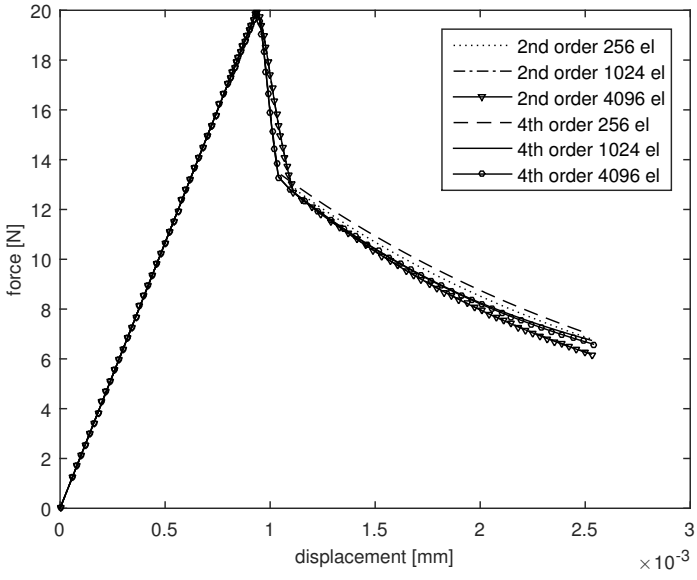

Figure 14. Load-displacement curves for square panel.

Moreoever, this corroborates the results of the dispersion analysis which indicate that the second-order formulation has a bigger band width. Conversely, for explicit gradient plasticity formulations, shear localisation analyses [33, 34] show a broader localisation band for an explicit second-order gradient model compared to an explicit gradient model with fourth-order gradients.

Figure 17 presents the evolution of the local and the nonlocal effective plastic strains. The second-order formulation with a mesh of 256 elements is employed. After localisation at $\bar{u} = 0.00096\,\mathrm{mm}$,

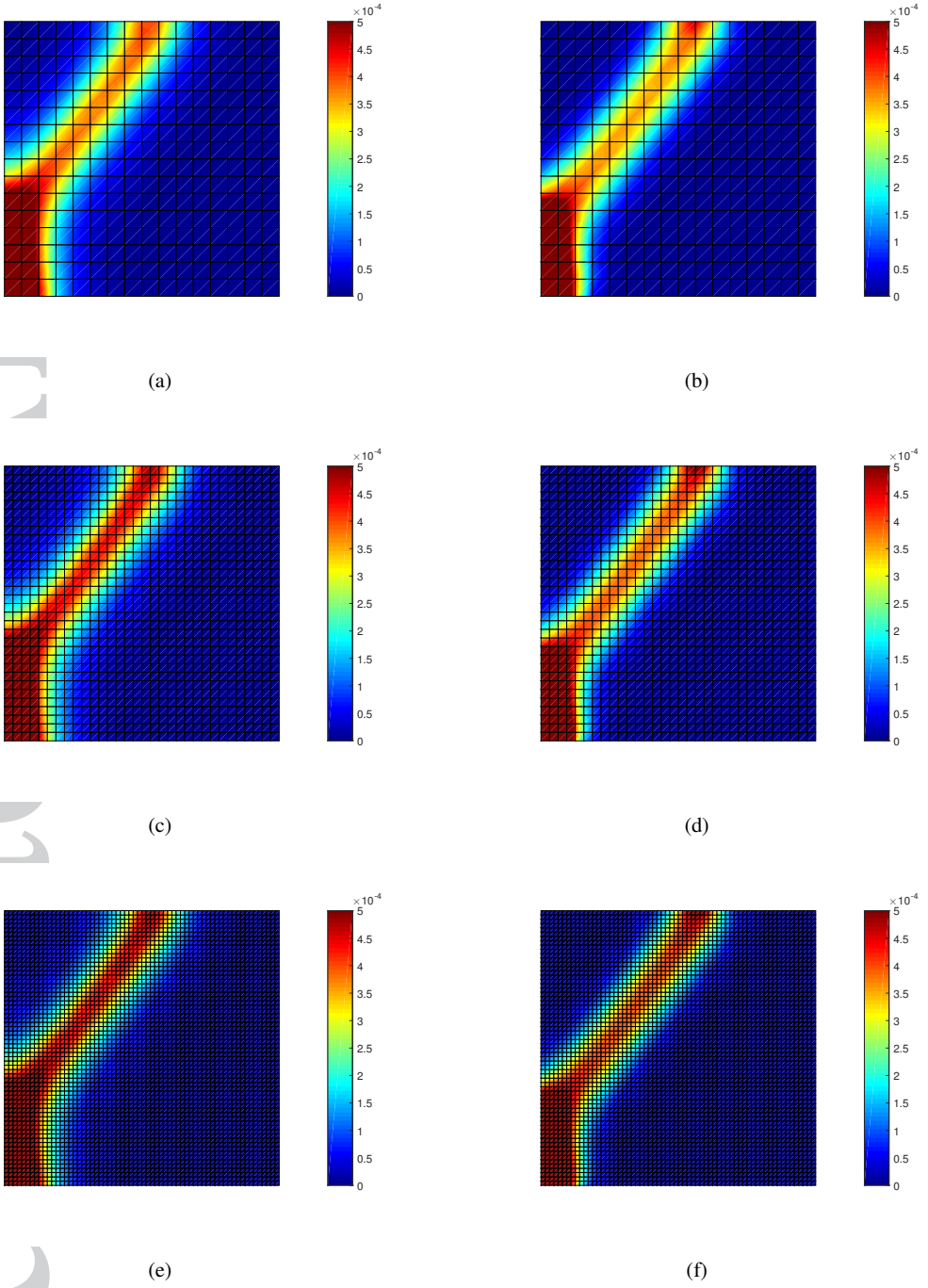

Figure 15. Square panel: Distribution of nonlocal effective plastic strain for the second-order (*left*) and fourth-order (*right*) formulations

.

further localisation within the band is observed in Figures 17(e) and 17(f). This is in agreement with results from standard finite element simulations [8].

Figures 15 and 17 indicate that the localisation zone first propagates along the vertical boundary before evolving into a shear band. This is consistent with earlier calculations for explicit and

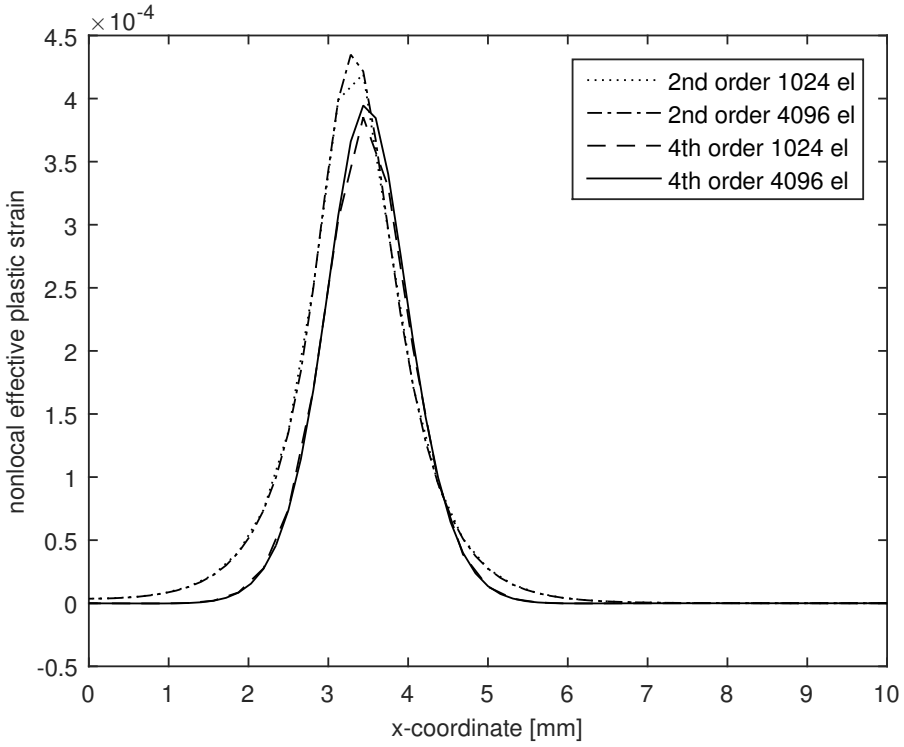

Figure 16. Distribution of nonlocal effective plastic strain along the diagonal AB, cf. Figure 12

implicit gradient plasticity models using standard finite elements [8], meshless methods [13] and isogeometric analysis [14]. The angle of the shear band is lower than 45° which is the theoretical solution for a shear band when using a Tresca plasticity model. Unlike for the Tresca yield function, the intermediate principal stress enters the Von Mises yield condition, and this results in a different condition for the onset of localisation, including the angle of shear bands, cf. [35]. It is finally noted that the curving upward of the shear band near the free boundary is related to the emergence of stationary Rayleigh waves [36], and has been observed in other simulations as well [37].

6.3. Biaxially compressed specimen

To further assess the capability of the model, a biaxially compressed plane-strain specimen is considered, Figure 18, cf. [12, 8]. The width $L = 10$ mm. All material parameters are as in the previous section except that now $\beta = 2500$ and $\nu = 0.3$. The elements with reduced yield strength (by 5%) are shown in Figure 19.

The load-displacement curves are shown in Figure 20. It is noted that for the second-order formulation, the load-displacement curve (after the cusp) has not fully converged with 200 elements. This is because the smallest element size (1 mm) is larger than the length scale considered [14]. However, the fourth-order formulation shows convergence, which may suggest a stronger regularisation property for the fourth-order formulation. The nonlocal effective plastic strains are plotted in Figure 21. No mesh dependency is observed.

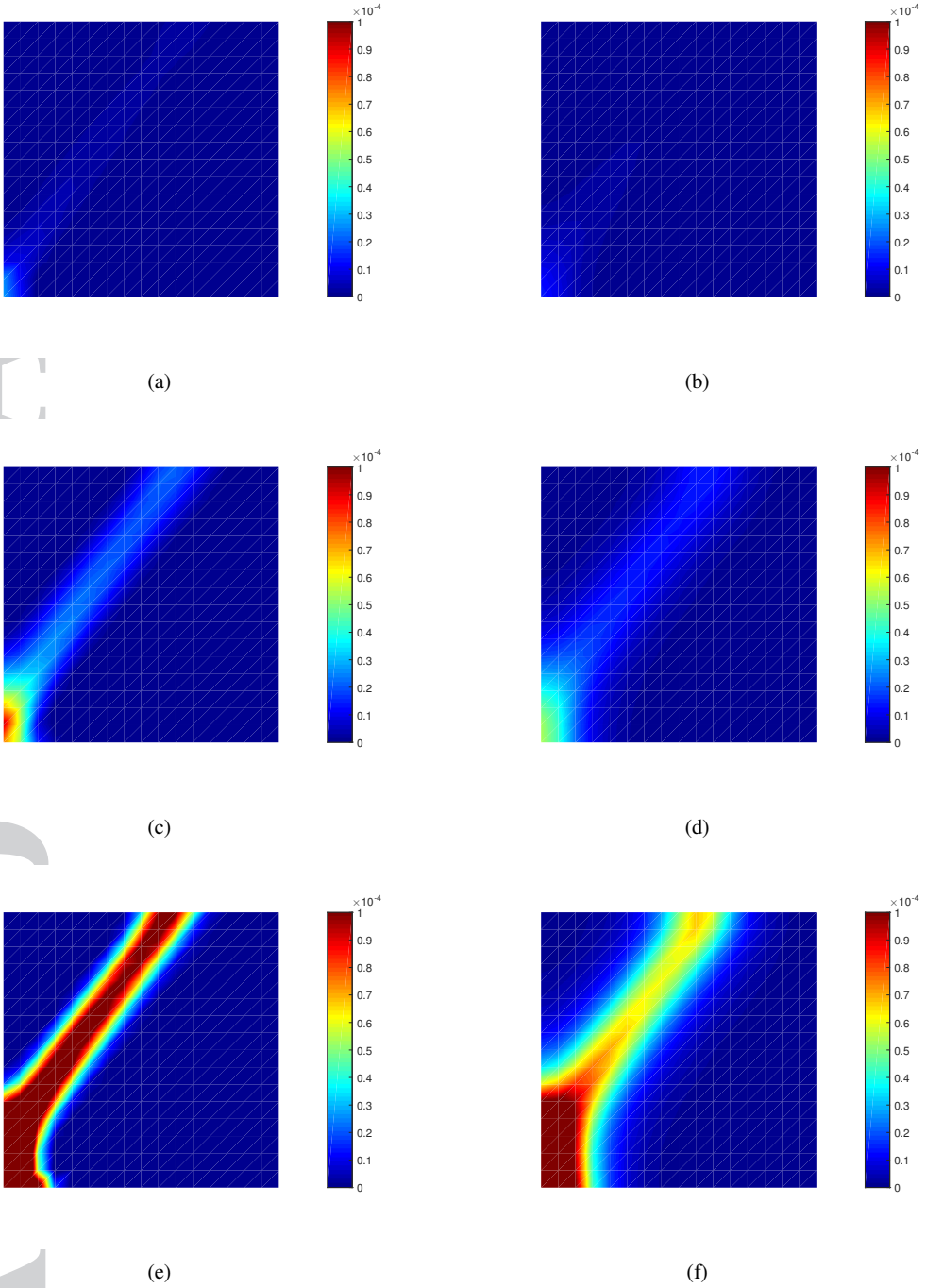

Figure 17. Evolution of the local (*left*) and the nonlocal (*right*) effective plastic strain at maximum displacement: $\bar{u} = 0.00093$ mm – (a), (b); $\bar{u} = 0.00096$ mm – (c), (d); $\bar{u} = 0.001$ mm – (e), (f)

.

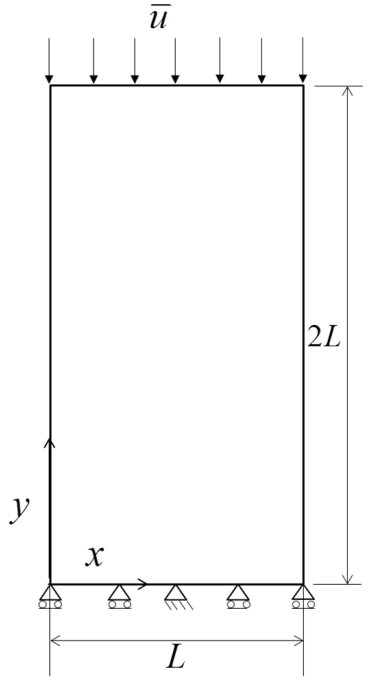

Figure 18. Biaxially compressed specimen: (a) geometry and boundary.

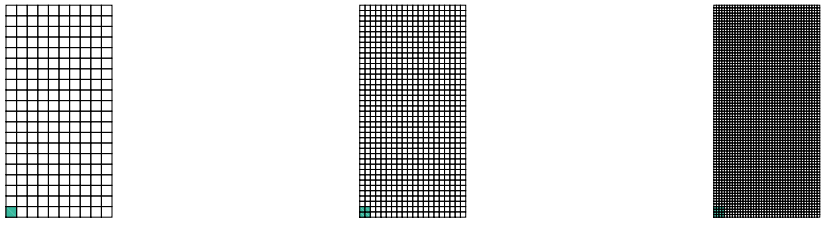

(a) (b) (c)

Figure 19. Mesh sizes and weakened elements for biaxially compressed specimen: (a) 200 elements; (b) 800 elements; (c) 3200 elements

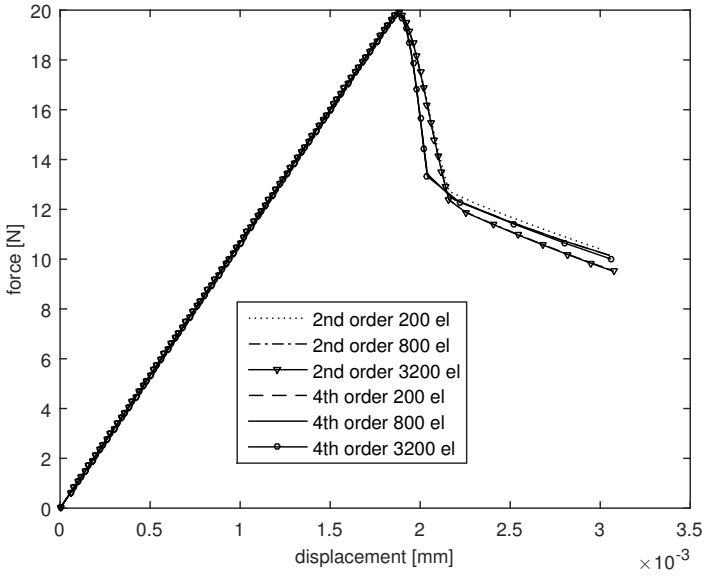

Figure 20. Load-displacement curves for biaxial compression test.

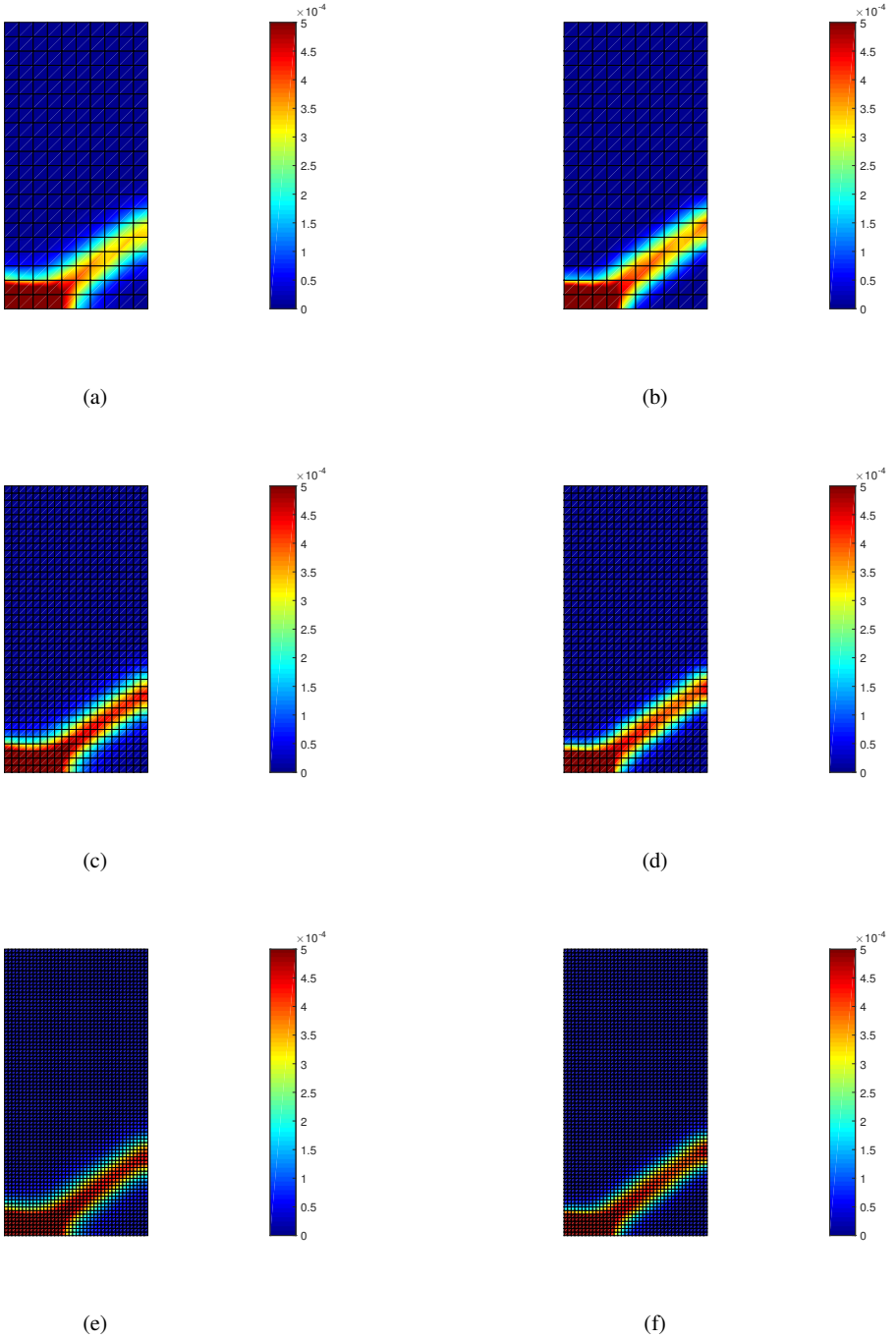

Figure 21. Biaxial compression: Distribution of nonlocal effective plastic strain for the second-order (*left*) and fourth-order (*right*) formulations.

.

7. CONCLUDING REMARKS

The introduction of strain softening in plasticity models leads to a loss of well-posedness of the boundary value problem. Various approachs to regularise the problem exist, such as the use of nonlocal models, either in an integral sense by spatial averaging, or in a differential sense, by including higher-order spatial gradients of a history variable. It is now well established that both approaches are closely related [10].

Computationally, the addition of gradients is preferred, since in this approach a sparse, banded stiffness matrix is preserved, and it is possible to retain symmetry of the tangential stiffness matrix, which is different from nonlocal integral approaches [38]. Explicit second-order gradient plasticity models properly regularise the boundary value problem, as has been shown by dispersion analyses, and one-dimensional and two-dimensional finite element analyses of localisation. However, in explicit gradient plasticity the interpolation of the plastic multiplier must satisfy $\mathcal{C}^1$-continuity, since this is a necessary condition at the moving, internal elasto-plastic boundary [3]. This degree of continuity is difficult to satisfy using finite element approaches, and alternative formulations have been put forward [12, 13, 14].

The use of a second-order implicit gradient plasticity model, in which the nonlocal plastic strain is interpolated [8], is an alternative way to solve this issue since a $\mathcal{C}^0$-continuous interpolation for the nonlocal plastic equivalent strain suffices. However, it does not rigorously regularise the boundary value problem [17]. In this paper we have explored the use of a fourth-order implicit gradient plasticity model. A dispersion analysis and one-dimensional and two-dimensional numerical analyses show that a regularisation, with mesh-independent results, can be obtained. Unfortunately, as with the explicit second-order gradient plasticity model, this requires a $\mathcal{C}^1$-continuous interpolation, now for the nonlocal plastic strain. Herein, it has been proposed to exploit isogeometric finite element analysis to meet this requirement.

It depends on the chosen damage relation whether the width of the localisation band tends to zero, thus resulting in a sharp crack, but also in a local loss of ellipticity. This is not different from the situation for second-order implicit gradient plasticity, but marks a clear difference with that for the second-order explicit gradient-plasticity model.

Finally, it is noted that for the present class of problems, an equal-order interpolation for both types of variables, displacements and (nonlocal) equivalent plastic strains, is sufficient, with the advantages that come when considering adaptive or hierarchical meshing.

APPENDIX A

Box 1. Algorithm for implicit gradient plasticity formulations (iteration $j+1$)

1. Compute the matrices $\mathbf{K}_{aa}$, $\mathbf{K}_{a\lambda}$, $\mathbf{K}_{\lambda a}$ and $\mathbf{K}_{\lambda\lambda}$, and forces $\mathbf{f}_e$, $\mathbf{f}_a$ and $\mathbf{f}_\lambda$, according to Equations (69) – (74)
2. Solve for $\mathrm{d}\mathbf{a}$ and $\mathrm{d}\bar{\mathbf{\Lambda}}$ using Equation (68)
3. Update the total increments $\Delta\mathbf{a}_{j+1} = \Delta\mathbf{a}_j + \mathrm{d}\mathbf{a}$, and $\Delta\mathbf{\Lambda}_{j+1} = \Delta\mathbf{\Lambda}_j + \mathrm{d}\mathbf{\Lambda}$.
4. Compute the following at each integration point:
   $\Delta\boldsymbol{\varepsilon}_{j+1} = \mathbf{B}\Delta\mathbf{a}_{j+1}$,
   $\Delta\bar{\lambda}_{j+1} = \mathbf{h}^{\mathrm{T}}\Delta\bar{\mathbf{\Lambda}}_{j+1}$,
   $\nabla(\Delta\lambda_{j+1}) = \mathbf{Q}^{\mathrm{T}}\Delta\mathbf{\Lambda}_{j+1}$,
   $\nabla^2(\Delta\lambda_{j+1}) = \mathbf{p}^{\mathrm{T}}\Delta\mathbf{\Lambda}_{j+1}$,
   $\bar{\kappa}_{j+1} = \bar{\kappa}_0 + \Delta\lambda_{j+1}$,
   $\nabla\bar{\kappa}_{j+1} = \nabla\bar{\kappa}_0 + \nabla(\Delta\bar{\lambda}_{j+1})$,
   $\nabla^2\bar{\kappa}_{j+1} = \nabla^2\bar{\kappa}_0 + \nabla^2(\Delta\bar{\lambda}_{j+1})$,
   compute ω_{j+1} according to adopted damage evolution law
   trial stress $\boldsymbol{\sigma}_t = \boldsymbol{\sigma}_0 + \mathbf{D}^e\Delta\boldsymbol{\varepsilon}_{j+1}$.
   If $F(\boldsymbol{\sigma}_t, \kappa_0, \bar{\kappa}_{j+1}) > 1\times10^{-6}$,
      then plastic state:
         compute $\mathbf{m}_t$
         compute $\Delta\gamma_{j+1}$
         $\kappa_{j+1} = \kappa_0 + \Delta\gamma_{j+1}$,
         compute the algorithmic stiffness operator $\mathbf{A}$
         update the trial stress update according to Equation (38)
   else
      elastic state:
         $\mathbf{m}_t = \mathbf{0}$
         $\boldsymbol{\sigma}_{j+1} = \boldsymbol{\sigma}_t$
         $\mathbf{A} = \mathbf{D}^e$
5. Check the global convergence criterion. If not converged, go to 1.

$(\bullet)_0$ denotes value at previous converged load step and $(\bullet)_j$ indicates value at previous iteration.

REFERENCES

1. Zdeněk P Bažant, Ted B Belytschko, and Ta-Peng Chang. Continuum theory for strain-softening. *Journal of Engineering Mechanics*, 110:1666–1692, 1984.
2. Zdeněk Bažant and Feng-Bao Lin. Non-local yield limit degradation. *International Journal for Numerical Methods in Engineering*, 26:1805–1823, 1988.
3. René de Borst and Hans-Bernd Mühlhaus. Gradient-dependent plasticity: Formulation and algorithmic aspects. *International Journal for Numerical Methods in Engineering*, 35:521–539, 1992.
4. H-B Mühlhaus and E C Alfantis. A variational principle for gradient plasticity. *International Journal of Solids and Structures*, 28:845–857, 1991.
5. R de Borst, L J Sluys, H-B Mühlhaus, and Jerzy Pamin. Fundamental issues in finite element analyses of localization of deformation. *Engineering Computations*, 10:99–121, 1993.
6. R H J Peerlings, R de Borst, W A M Brekelmans, and J H P de Vree. Gradient enhanced damage for quasi-brittle materials. *International Journal for Numerical Methods in Engineering*, 39:3391–3403, 1996.
7. Harm Askes, Jerzy Pamin, and René de Borst. Dispersion analysis and element-free Galerkin solutions of second- and fourth-order gradient-enhanced damage models. *International Journal for Numerical Methods in Engineering*, 49:811–832, 2000.
8. Roy A B Engelen, Marc G D Geers, and Frank P T Baaijens. Nonlocal implicit gradient-enhanced elasto-plasticity for the modelling of softening behaviour. *International Journal of Plasticity*, 19:403–433, 2003.
9. Clemens V Verhoosel, Michael A Scott, Thomas J R Hughes, and René de Borst. An isogeometric analysis approach to gradient damage models. *International Journal for Numerical Methods in Engineering*, 86:115–134, 2011.

10. R H J Peerlings, M G D Geers, R de Borst, and W A M Brekelmans. A critical comparison of nonlocal and gradient-enhanced softening continua. *International Journal of Solids and Structures*, 38:7723–7746, 2001.
11. T. H. A. Nguyen, T. Q. Bui, and S. Hirose. Smoothing gradient damage model with evolving anisotropic nonlocal interactions tailored to low-order finite elements. *Computer Methods in Applied Mechanics and Engineering*, 328:498–541, 2018.
12. Rene de Borst and Jerzy Pamin. Some novel developments in finite element procedures for gradient-dependent plasticity. *International Journal for Numerical Methods in Engineering*, 39:2477–2505, 1996.
13. Jerzy Pamin, Harm Askes, and René de Borst. Two gradient plasticity theories discretized with the element-free Galerkin method. *Computer Methods in Applied Mechanics and Engineering*, 192:2377–2403, 2003.
14. I. Kolo and R. de Borst. An isogeometric analysis approach to gradient plasticity. *International Journal for Numerical Methods in Engineering*, DOI: 10.1002/nme.5614.
15. R de Borst, J Pamin, R H J Peerlings, and L J Sluys. On gradient-enhanced damage and plasticity models for failure in quasi-brittle and frictional materials. *Computational Mechanics*, 17:130–141, 1995.
16. Giovanni Di Luzio and Zdeněk P Bažant. Spectral analysis of localization in nonlocal and over-nonlocal materials with softening plasticity or damage. *International Journal of Solids and Structures*, 42:6071–6100, 2005.
17. L H Poh and S Swaddiwudhipong. Gradient-enhanced softening material models. *International Journal of Plasticity*, 25:2094–2121, 2009.
18. Xilin Lu, Jean-Pierre Bardet, and Maosong Huang. Spectral analysis of nonlocal regularization in two-dimensional finite element models. *International Journal for Numerical and Analytical Methods in Geomechanics*, 36:219–235, 2012.
19. Milan Jirásek and Simon Rolshoven. Comparison of integral-type nonlocal plasticity models for strain-softening materials. *International Journal of Engineering Science*, 41:1553–1602, 2003.
20. Milan Jirásek and Simon Rolshoven. Localization properties of strain-softening gradient plasticity models. Part II: Theories with gradients of internal variables. *International Journal of Solids and Structures*, 46:2239–2254, 2009.
21. R A B Engelen, N A Fleck, R H J Peerlings, and M G D Geers. An evaluation of higher-order plasticity theories for predicting size effects and localisation. *International Journal of Solids and Structures*, 43:1857–1877, 2006.
22. Thomas J R Hughes, John A Cottrell, and Yuri Bazilevs. Isogeometric analysis: CAD, finite elements, NURBS, exact geometry and mesh refinement. *Computer Methods in Applied Mechanics and Engineering*, 194:4135–4195, 2005.
23. Michael J Borden, Michael A Scott, John A Evans, and Thomas J R Hughes. Isogeometric finite element data structures based on Bézier extraction of NURBS. *International Journal for Numerical Methods in Engineering*, 87:15–47, 2011.
24. R. de Borst, M. A. Crisfield, J. J. C. Remmers, and C. V. Verhoosel. *Non-linear Finite Element Analysis of Solids and Structures*. John Wiley & Sons, Chichester, second edition, 2012.
25. R H J Peerlings, R de Borst, W A M Brekelmans, J H P de Vree, and I Spee. Some observations on localisation in non-local and gradient damage models. *European Journal of Mechanics A: Solids*, 15:937–953, 1996.
26. Gerald Beresford Whitham. *Linear and Nonlinear Waves*. John Wiley & Sons, New York, 1974.
27. L J Sluys, R de Borst, and H-B Mühlhaus. Wave propagation, localization and dispersion in a gradient-dependent medium. *International Journal of Solids and Structures*, 30:1153–1171, 1993.
28. L J Sluys and R de Borst. Dispersive properties of gradient-dependent and rate-dependent media. *Mechanics of Materials*, 18:131–149, 1994.
29. M. G. Cox. The numerical evaluation of B-splines. *IMA Journal of Applied Mathematics*, 10:134–149, 1972.
30. C. de Boor. On calculating with B-splines. *Journal of Approximation Theory*, 6:50–62, 1972.
31. Julien Vignollet, Stefan May, and René de Borst. Isogeometric analysis of fluid-saturated porous media including flow in the cracks. *International Journal for Numerical Methods in Engineering*, 108:990–1006, 2016.
32. A Simone, H Askes, R H J Peerlings, and L J Sluys. Interpolation requirements for implicit gradient-enhanced continuum damage models. *International Journal for Numerical Methods in Biomedical Engineering*, 19:563–572, 2003.
33. A Menzel and P Steinmann. On the continuum formulation of higher gradient plasticity for single and polycrystals. *Journal of the Mechanics and Physics of Solids*, 48:1777–1796, 2000.
34. Xue-Bin Wang. Adiabatic shear localization for steels based on Johnson-Cook model and second- and fourth-order gradient plasticity models. *Journal of Iron and Steel Research, International*, 14:56–61, 2007.
35. J. W. Rudnicki and J. R. Rice. Conditions for the localization of deformation in pressure-sensitive dilatant materials. *Journal of the Mechanics and Physics of Solids*, 23:371–394, 1975.
36. A. Needleman and M. Ortiz. Effect of boundaries and interfaces on shear-band localization. *International Journal of Solids and Structures*, 28:859–877, 1991.
37. R. de Borst, J. Réthoré, and M. A. Abellan. A numerical approach for arbitrary cracks in a fluid-saturated medium. *Archive of Applied Mechanics*, 75:595–606, 2006.
38. G. Pijaudier-Cabot and A. Huerta. Finite element analysis of bifurcation in nonlocal strain softening solids. *Computer Methods in Applied Mechanics and Engineering*, 90:905–919, 1991.